TU Delft

Linear analysis of thermal inertia effects on the thermal-hydraulic stability of a natural circulation driven supercritical water loop

G.I.A. Lippens
February 18, 2014
NERA-131-2014-001

Bachelor of Science thesis

Supervisor:	Dr. ir. M. Rohde	
Committee:	Dr. ir. M. Rohde	Delft University of Technology, Faculty of Applied Sciences
	Dr. ir. D. Lathouwers	Delft University of Technology, Faculty of Applied Sciences

Delft,
February 18, 2014

Delft University of Technology
Faculty of Applied Sciences
Dept. of Radiation Science and Technology
Sect. Nuclear Energy and Radiation Applications

ABSTRACT

The Supercritical Water-cooled Reactor (SCWR) is one of the six nuclear reactors proposed by the Generation IV International Forum and is based on Light Water Reactor technology. The SCWR can be designed such that the removal of heat from the core can occur through natural circulation, rather than through the use of active pumps, thereby making the reactor more inherently safe. This thesis extends an existing computational model for calculating unstable operational conditions for the natural circulation-driven SCWR, by implementing the effect of the thermal inertia of the core wall.

The model is configured by setting up conservation balances (mass, heat and momentum) for a handful of nodes, to which the reactor is simplified. The balance equations are linearized using Taylor expansion, so that the problem can be written as a time-dependent matrix-vector equation, effectively reducing the system to an eigenvalue problem. For setting up the coefficient matrix the steady state solutions to the conservation balances are needed and these are found through an iterative process.

It is found that the implementation of the wall has a generally stabilizing effect, but as the cross-sectional area of the wall is enlarged, the stability declines. Several previously unseen instability regimens emerge as well. Similarities are found between the computed stability boundary and earlier results from experiments with supercritical Freon R23.

The thesis includes frequency studies to determine the dominant underlying mechanisms driving the instabilities, as well as a brief study of Ledinegg instabilities.

TABLE OF CONTENTS

1. INTRODUCTION

1.1 Background

Along with the rapidly increasing global energy demand comes the need for innovative solutions. Scientists and engineers worldwide search for energy technologies that are cleaner, more reliable and less costly than the combustion of fossil fuels, the globally dominant source of energy. One of the most promising alternatives is nuclear reactor technology, which is estimated to already save 2.5 billion tonnes from being on top of the 8 billion tonnes of CO_2 currently emitted each year (Ortega Gómez, 2009). The *Nuclear Energy and Radiation Applications* (NERA) section of Delft University of Technology performs research on reactor technology.

The Generation IV International Forum has selected six possible reactor types for further study. These are the gas-cooled fast reactor (GFR), the very-high-temperature reactor (VHTR), the sodium-cooled fast reactor (SFR), the lead-cooled fast reactor (LFR), the molten salt reactor (MSR) and the supercritical water-cooled reactor (SCWR) types. These reactor types are commonly referred to as Generation IV reactor types, with the advantages of being less costly, more proliferation-resistant and inherently safe and less waste-producing (Generation IV International Forum, viewed 2013).

This thesis focuses on the High Performance Light Water Reactor (HPLWR), a European Union-based R&D program on the SCWR concept. The reactor has a projected power output around 1000 MW and its thermal efficiency is about 45%, compared to 33% of today's operational LWR systems (Ortega Gómez, 2009). Like the conventional BWR and PWR systems, the SCWR system uses light water as both coolant and neutron moderator. The reactor pressure is 25 MPa, which lies above the thermodynamic critical point –further explanation in section 1.2.. This allows for the system to operate on a much broader temperature range than its 'predecessors' , the BWR and PWR systems. Another advantage lies in the possibility of utilizing both thermal- and fast-spectrum neutrons, thereby reducing the production of minor actinides. (Generation IV International Forum, viewed 2014)

The Nuclear Energy and Radiation Applications (NERA) group of Delft University of Technology investigates a natural circulation driven version of the HPLWR, in which the coolant flow is driven by gravitational pressure drops, rather than by pumps. This feature adds to the inherent safety of the reactor.

1.2 High Performance Light Water Reactor

The HPLWR is based on the SCWR concept. In Figure 1.1 a schematic overview of the SCWR is shown. As the water enters the core it is in a liquid state. The pressure inside the reactor pressure vessel is constantly kept above the critical pressure of 22.064 MPa, so that the water, as it is heated in the core, passes maximum specific heat capacity and becomes supercritical. The temperature at which the heat capacity reaches its maximum value is referred to as the pseudo-critical temperature. The heat is then converted to work in a turbine, which drives a generator, and the relatively small quantity of remaining heat is exchanged using a condenser.

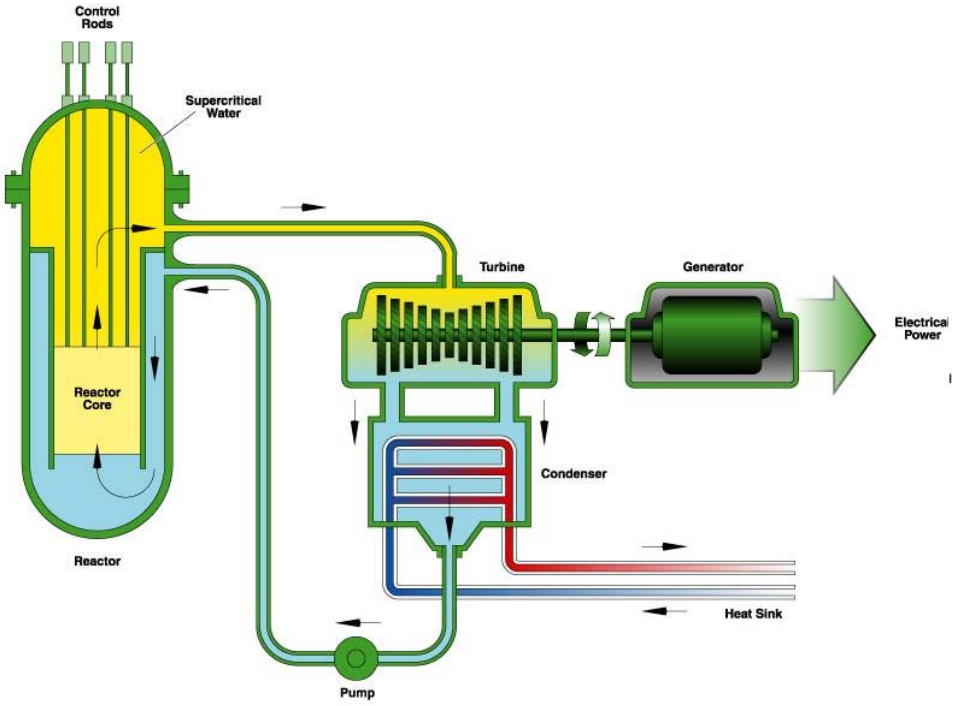

Figure 1.1. Schematic overview of the SCWR (GEN-IV, 2013).

Like the BWR and unlike the PWR, the SCWR uses only a single loop for heat transfer. In this figure the pump ensures a constant coolant flow. The phase diagram in Figure 1.2 shows the temperature range and pressure at which the HPLWR is to operate.

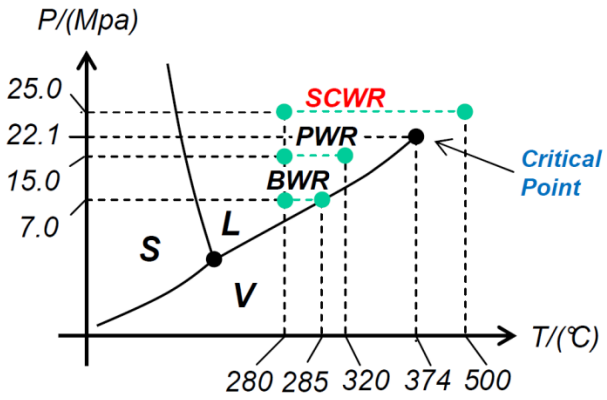

Figure 1.2. PT-diagram displaying temperature ranges for several LWR types (Spoelstra, 2012).

Supercriticality is shown in the PT-diagram as the range of all points with both a higher pressure and higher temperature than the critical point. When liquid matter is heated at supercritical pressure, and, when it is heated towards a certain pseudo-critical point, it displays behaviour similar to that of water near the boiling point. While for a subcritical fluid at the boiling point the rapid changes in density, viscosity, etc. occur very abruptly with a small change in enthalpy though, the similar changes occur more gradually in the phase transition from liquid to supercritical. This is shown in Figure 1.3.

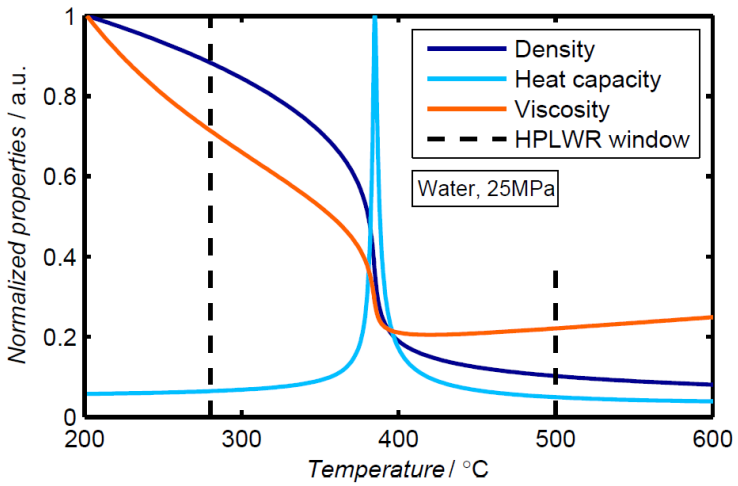

Figure 1.3. Development of water density, specific heat capacity and dynamic viscosity versus temperature at p = 25 MPa (Spoelstra, 2012).

The core of the HPLWR will be divided into three heating phases, separated by two mixing plena in order to prevent local temperature extremes that can damage the core internals (Ortega Gómez, 2009). When the coolant enters the core at about 310°C it will be heated up in the 'evaporator' phase, past the pseudo-critical temperature (hence probably the reference to evaporation, even though technically no vapour is formed) to a temperature of 390°C and consequently through the 'superheaters' I and II, which will heat the coolant up to temperatures of 435°C and 500°C respectively, as is shown in Figure 1.4.

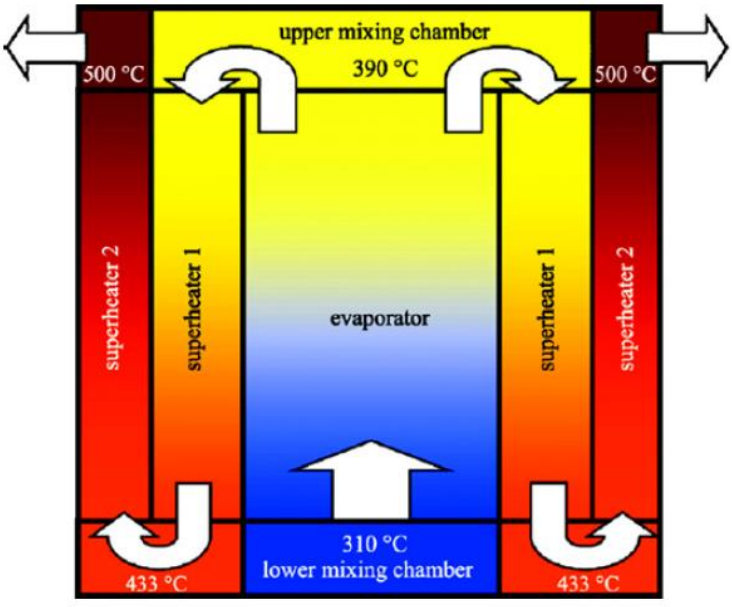

Figure 1.4. Schematic display of the three-stage heating plan in the core of the HPLWR (T'Joen & Rohde, 2012).

The HPLWR may be designed to rely less on active pumps for coolant circulation, by placing a riser above the core, enabling coolant flow by natural convection. In Figure 1.3 can be seen that the density of the coolant drops significantly around the pseudo-critical point. Consequently a gravitational

pressure drop is created, which drives the circulation. The addition of the riser enhances this natural circulation (Krijger, 2013). Less reliance on active systems is considered more inherently safe, as the failure of active systems leaves the heat with no way to go, eventually resulting in core damage.

Placing a riser above the core is not a particularly new idea. In the past NERA researched the dynamics of natural circulation-driven BWR systems, such as the Economic Simplified Boiling Water Reactor (ESBWR) by GE Hitachi (Van Bragt, 1998).

1.3 Stability issues

A system is called stable if it responds to a small perturbation by returning to the state it was in before the perturbation occurred. Ortega Gómez (2009) describes various types of instabilities for SCWR systems in his dissertation. Following the proposal of Bouré et al (1973), he distinguishes static from dynamic instabilities. The former can be explained using the steady-state equations of the system, whereas the latter are explained by transient behaviour, caused by feedback mechanisms.

One example of static instabilities is the Ledinegg instability. This type of instability occurs as the mass flow suddenly changes between (steady-state) values. When the coolant flow in the system can attain multiple values in steady state, a small perturbation can lead to the flow suddenly switching between these. Krijger (2013) developed a method for finding Ledinegg instabilities in natural convection driven supercritical water loops numerically. This method is made possible due to the characteristic shown in Figure 1.5.

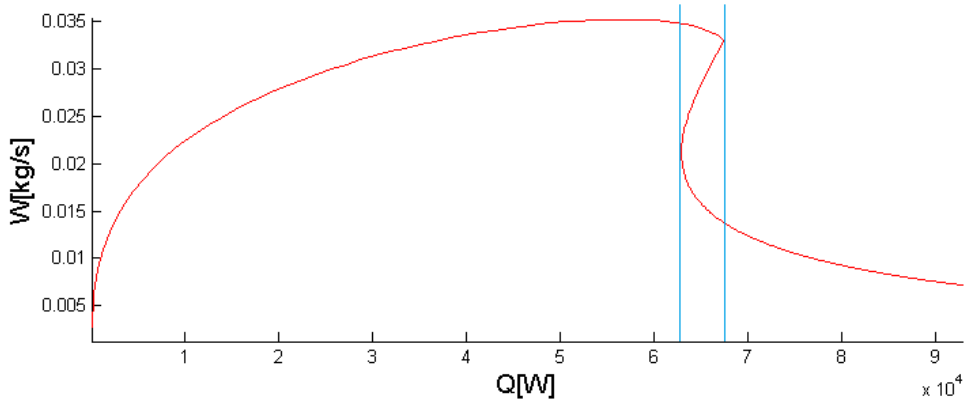

Figure 1.5. Flow rate to heating power characteristic for a given inlet temperature. The Ledinegg unstable region is bordered by the vertical turquoise lines.

Dynamic instabilities in natural circulation driven BWR systems are further divided in type I and II dynamic instabilities by Van Bragt (1998), the former being due to gravitational pressure drop in the riser section and resulting in low-frequency oscillations. The latter occur due to frictional pressure losses and oscillate at a higher frequency (Koren, 2010), generally around 0.1 Hz (Krijger, 2013). These oscillations are mainly caused by local density differences and consequently, they are commonly referred to as Density Wave Oscillations (DWO). The development of the amplitude over time is described by the Decay Ratio (DR). The DR is the base number in an exponential time function. A DR larger than unity denotes an unstable system, whereas for a stable system the DR is smaller than unity. Figure 1.6 shows two examples of the evolution of a perturbation, one with a DR smaller than unity, one with a DR larger.

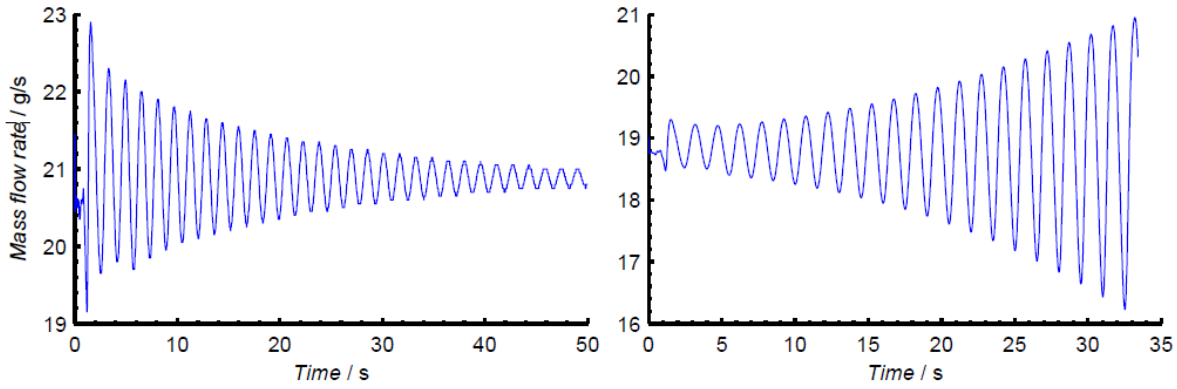

Figure 1.6. Typical time development of a perturbation with DR<1 (left) and one with DR>1 (right) (Spoelstra,2012).

The operational conditions of a LWR can be summarized by two dimensionless variables, one being a measure for the heat and mass flows – usually a ratio – the other being a measure for the temperature at the core inlet. Subsequently these variables can be used as axes to a map of stable and unstable operational conditions. The border between stable and unstable regions on such an instability map is called the Neutral Stability Boundary (NSB). One example of a Neutral Stability Boundary is shown in Figure 1.7.

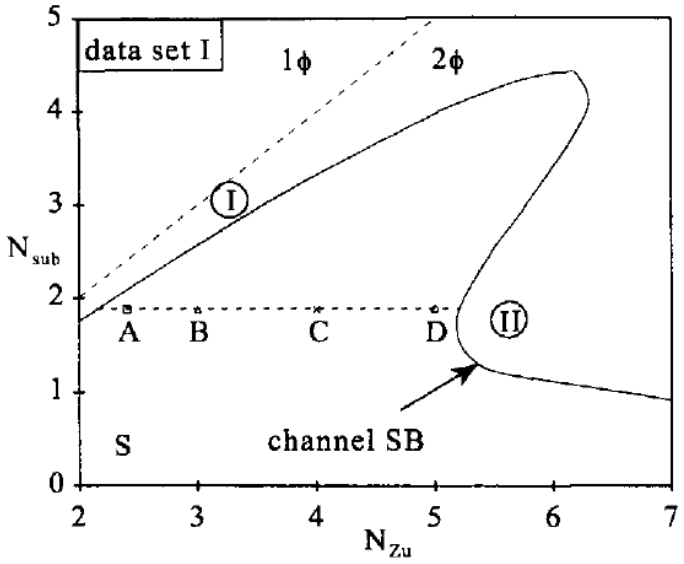

Figure 1.7. An instability map for a Boiling Water Reactor with Neutral Stability Boundary. The Roman numbers I and II indicate that the dynamic instabilities in their respective regions are type I and type II dynamic instabilities respectively (Van Bragt, 1998).

1.4 Literature

Natural circulation driven two-phase loops have been studied by Marcel (2007) and Van Bragt (1998), among others, of the Nuclear Energy and Radiation Applications group of Delft University of Technology.

Natural circulation supercritical loop experiments using CO_2 have been performed by Lomperski et al. (2004) but showed no agreement with the numerical results later obtained by Jain (2008). An experimental setup for investigating supercritical loop stability has been built at the TU Delft and was named DeLight – short for Delft Light Water Reactor Facility - using Freon R23, because of the relatively low pressure and temperature needed to attain supercriticality (T'Joen & Rohde, 2012). Kam (2011) and Spoelstra (2012) performed numerical research on the issue, but only partial agreement with the DeLight experiment was found. Schenderling (2013) included thermal inertia in Spoelstra's numerical model and found the upward trend in the rightmost NSB region, as well as the significance of the inclusion of the core wall to the stability. The NSB's found by Spoelstra and Schenderling are shown in Figure 1.8.

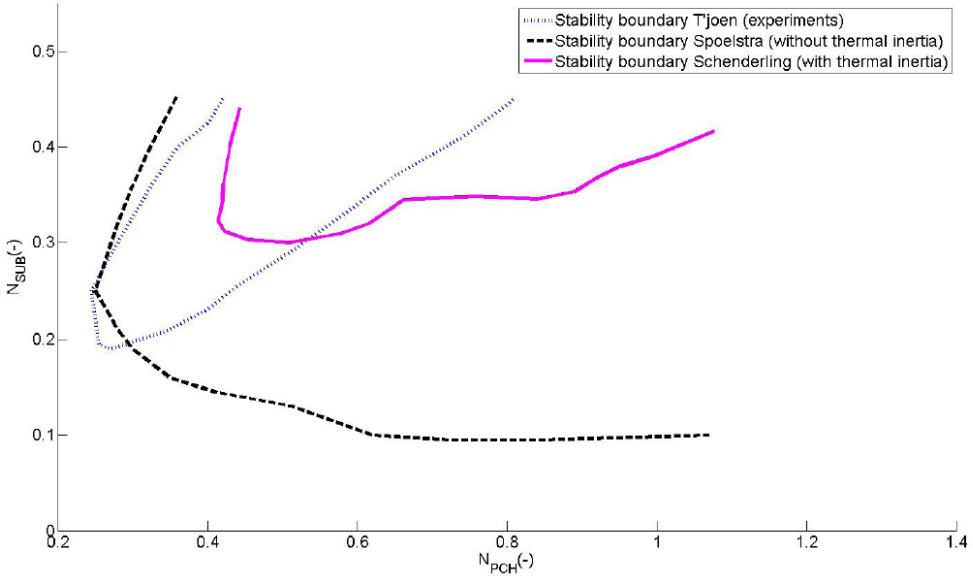

Figure 1.8. Experimental results of T'Joen & Rohde (2012), compared to the numerical results of Spoelstra (2012) and Schenderling (2013).

A simpler numerical analysis was performed by Krijger (2013) for a natural circulation driven supercritical water loop. In this qualitative analysis the loop is modelled consisting of four or five (depending on whether or not the pseudo-critical point is reached in the core) interacting nodes. Wall thermal inertia and neutronic-thermohydraulic coupling were not taken into account in this analysis. The steady state solutions of the governing equations are found through iteration and the stability is investigated by linearizing the transient governing equations and effectively reducing the equation system to an eigenvalue problem. Krijger performed a parametric study investigating the influence of various design parameters on the loop stability and found that the length of the riser destabilized the system, whereas conversely the volume of a buffer vessel included in the model showed to correlate positively with the loop stability.

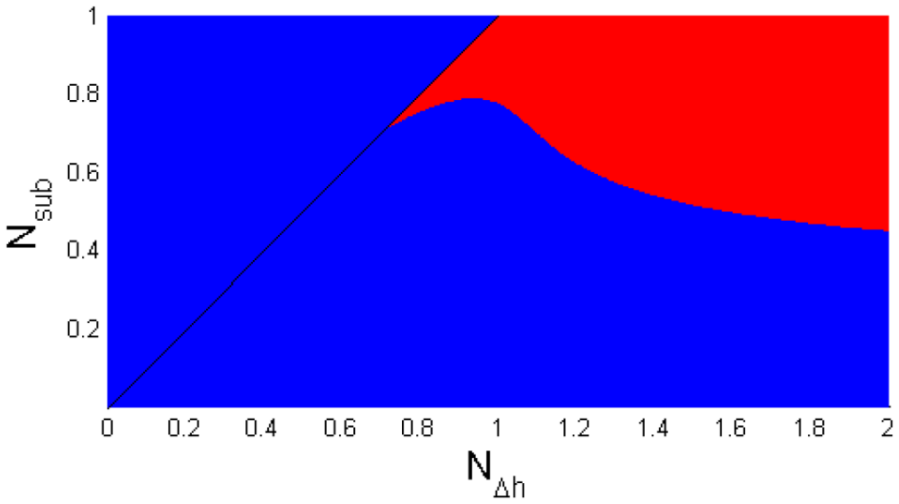

Figure 1.9. Instability map resulting from Krijger's (2013) numerical model.

1.5 Thesis outline

This thesis extends Krijger's (2013) analysis by implementing the effects of core wall thermal inertia into the system.

In the next chapter an overview of the simplified system will be presented, along with the equation of state, through which coolant density, temperature and thermal conductivity will be modelled as a function of specific enthalpy alone. The governing equations will be formulated, made dimensionless and linearized. Emphasis will be placed on the core wall thermal inertia effects. The final part of Chapter 2 will focus on acquiring steady state solutions to the nonlinear equations and on solving the resulting system of equations as an eigenvalue problem.

Subsequently in Chapter 3 the computational algorithm through which the system is studied will be explained, specifically the acquisition of the steady state values and the solution to the eigenvalue problem.

Chapter 4 will present a stability map for a standard reference case and will include a parametric study on the influence of the wall's cross-sectional area and thermal conductivity as well as the channel cross-sectional area. The Ledinegg instabilities will briefly be discussed and the model will be compared to the case, would the thermal conductivity be considered constant.

Chapter 5 will finally draw some conclusions from the results and recommendations for further investigation will be made.

2. PHYSICAL MODELLING

2.1. System overview

Krijger (2013) investigated the qualitative behaviour of a natural convection supercritical water loop through an analytical model developed by Rohde, along the lines of a boiling water channel model by Guido et al. (1991). The most important feature in this model is that the core, in which the coolant is heated, is reduced to a single channel with constant specified hydraulic diameter D_h and flow area A, as is the riser that is placed on top of it. After passing the riser the coolant enters a buffer vessel, which represents the system of turbines and heat exchangers needed to cool down the coolant to the specified inlet temperature. The energy exchanged through this system is represented in Figure 2.1. by a single variable q. A downcomer, that has the same geometrical parameters as the core and riser, subsequently leads the coolant back into the core.

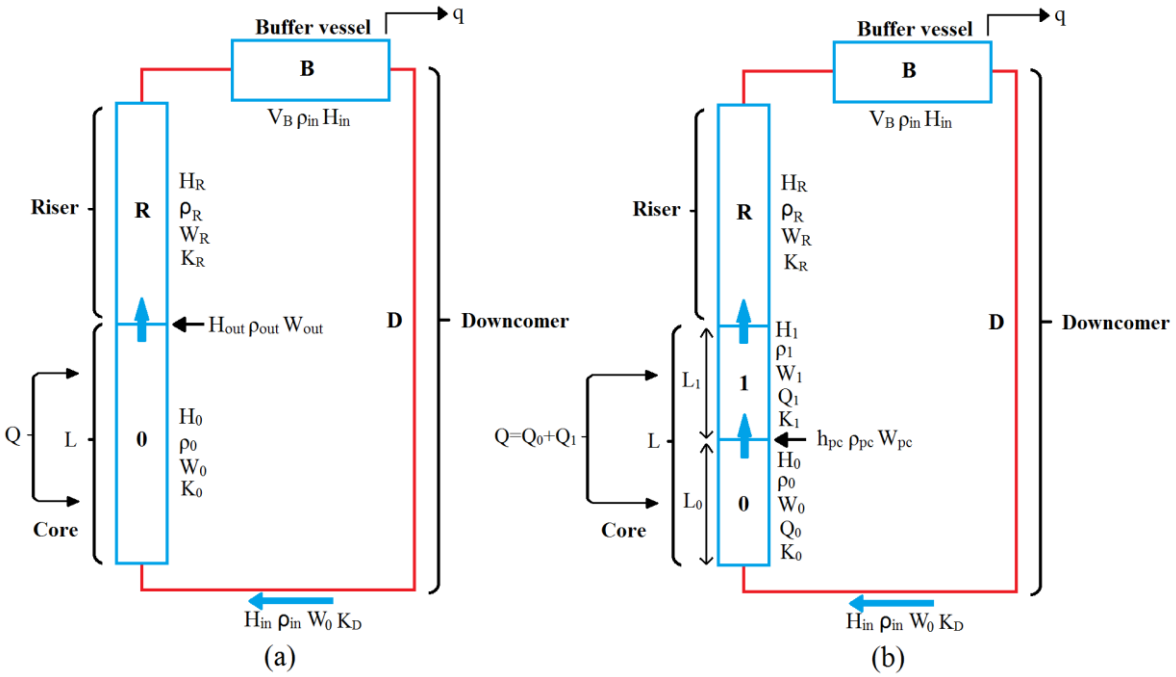

Figure 2.1. The supercritical water loop model (Krijger, 2013). The left figure shows the low-heating model, in which the pseudo-critical point is not reached in the core section. The right figure shows the high-heating model.

Around pseudo-critical enthalpy various properties of the coolant display highly nonlinear behaviour. For this reason in general different approximation schemes need to be used in order to model these properties correctly, as will be shown in section 2.2.. Consequently, the core itself is modelled as either one or two nodes, depending on whether or not pseudo-critical enthalpy is reached in the core. This leads to the models shown in Figure 2.1. The model with one core node, the one in which the coolant does not reach pseudo-critical enthalpy through core heating, will be referred to as the low-heating model. The two core node model will be referred to as – not so surprisingly – the high-heating model.

In Krijger's model, neither neutronic-thermo-hydraulic coupling nor core wall thermal inertia were taken into account. Here two additional nodes modelling the core wall are introduced. They are denoted *w0* and *w1*. The lengths of the wall nodes correspond to the lengths of the core nodes. In

Krijger's thesis, the heat flux to the core section of the channel is assumed constant and time-independent, as the heat Q is directly fed into the channel. In this model, the constant heat Q is no longer directly fed to the channel, but is fed to the wall and is then transferred to the channel. As a consequence of the thermal inertia of the wall, the heat transfer to the channel becomes time-dependent. In the high-heating model, through conduction, the wall nodes exchange heat among themselves as well, thereby closing a secondary feedback loop. The resulting models are shown in Figure 2.2.

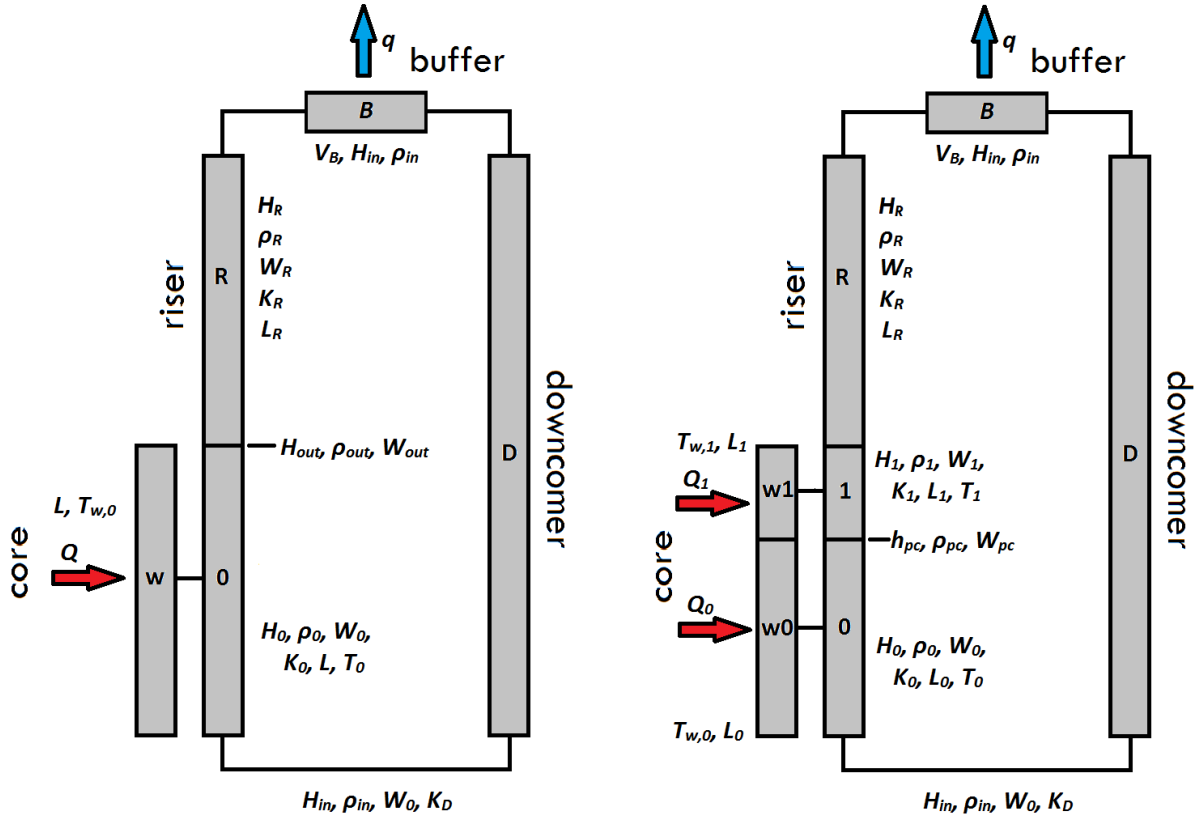

Figure 2.2. The model for the water loop including the effect of the thermal inertia of the core wall.

2.2. Equation of state

It is desired, for the sake of simplicity, that chemical properties of the coolant be considered dependent only on the local specific enthalpy of the coolant. This requires that the pressure is constant throughout the system. While gravitational and frictional pressure changes do occur, the assumption is made that these changes do not affect the specific enthalpy-dependent behaviour significantly. This justifies the assumption of constant pressure, which is taken 25 MPa. The equation of state is approximated using a two-region approach, pseudo-critical enthalpy being the border between the two of these.

The equation of state is used by Krijger (2013) for the modelling of the density of water as a function of enthalpy at 25 MPa. In the low enthalpy region the density is assumed to decrease linearly with enthalpy, as in the high enthalpy region, the specific volume, which is just inverse density, is assumed to increase linearly with enthalpy. The result is summarized in the equations and figures below. The

fitted values for the linearization constants in these equations equal C_1 = -4.7877 x_{10}^{-4} $kg^2m^{-3}J^{-1}$ and C_2 = 0.80 x_{10}^{-8} m^3J^{-1}.

$$v_i = \begin{cases} \frac{1}{\rho_{pc}+C_1(H_i-h_{pc})} & (H_i < h_{pc}) \\ v_{pc} + C_2(H_i - h_{pc}) & (H_i \geq h_{pc}) \end{cases} \tag{2.1}$$

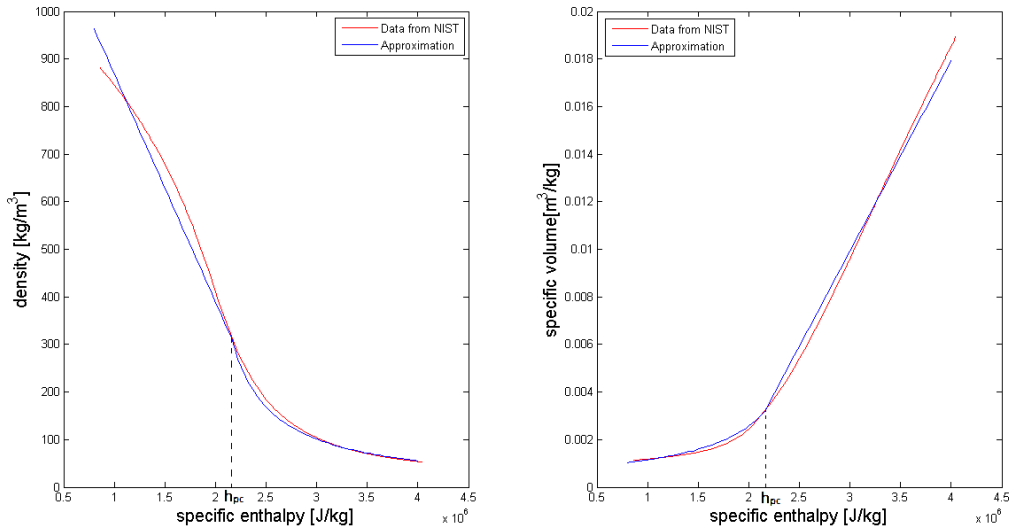

Figure 2.3. The specific volume approximation from the equation of state. Left shows the linearization of the density for the low-heating model, while the right figure displays a linearized specific volume for the high-heating model.

In this thesis, additionally, the temperature is approximated using quadratic functions in both regions, as quadratic functions offer the convenience of being linearized quite easily. Specific attention has been paid to ensure that the approximation and its slope are both continuous at pseudo-critical enthalpy. The temperature approximation can be expressed using a single equation:

$$T_i = \alpha_i(H_i - h_{pc})^2 + \frac{1}{c_{p,pc}}(H_i - h_{pc}) + T_{pc} \tag{2.2}$$

In this equation $c_{p,pc}$ is the specific heat of water at the pseudo-critical point of p=25 MPa, T_{pc} = 389°C. a_i has a value of a_0 = -1.1 x_{10}^{-10} KJ^{-2} in the low enthalpy region and a value of a_1 = 1.0 x_{10}^{-10} KJ^{-2} in the high enthalpy region. In Figure 2.4 the temperature is plotted against the enthalpy. The slope $\frac{dT}{dH}$ is the inverse of the enthalpy dependent specific heat $c_p(H)$ of the coolant – not to be confused with the specific heat $c_{p,pc}$ of the coolant at the pseudo-critical point. Note that enthalpy and temperature are coupled one-to-one, and therefore H can also be written unambiguously as a function of T.

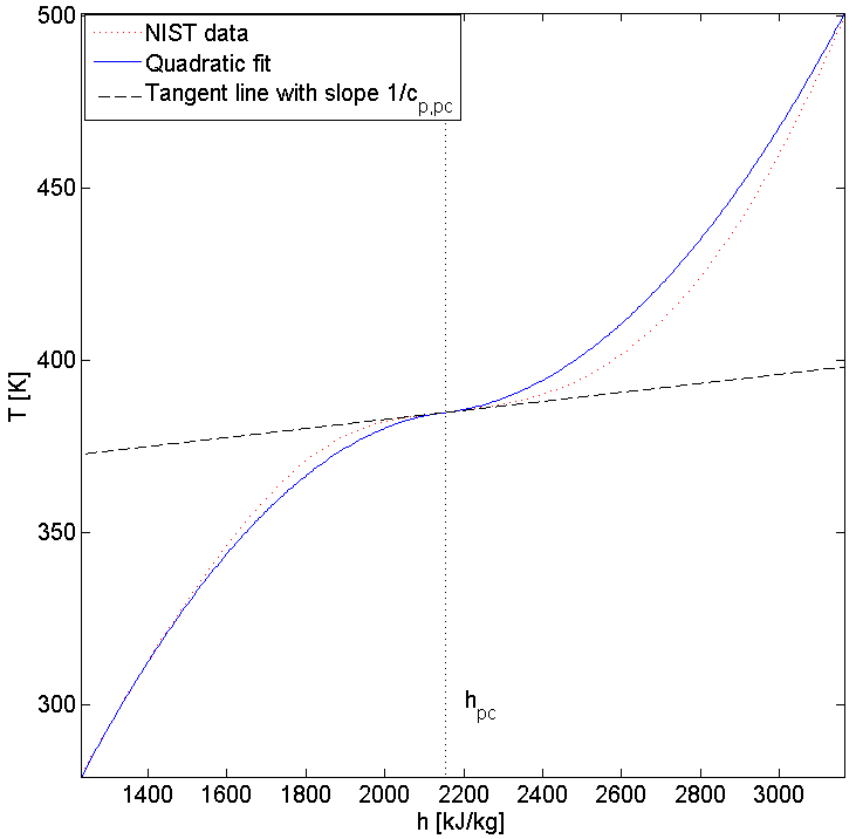

Figure 2.4. The temperature approximation from the equation of state. The red-dotted curve represents measurement data (NIST, 2013).

Finally, the thermal conductivity is modelled. The approximation of the thermal conductivity should, for simplicity reasons, loosely follow the trend of the actual thermal conductivity. In the low enthalpy region the thermal conductivity is approximated with a linear function and in the high enthalpy region with an exponential function.

$$\lambda_{f,0} = -\beta_0 H_0 + \lambda_{f,b,0} \tag{2.3a}$$

$$\lambda_{f,1} = \lambda_z e^{-\beta_1 H_1} + \lambda_{f,b,1} \tag{2.3b}$$

Equations (2.3a) and (2.3b) together require five additional parameter values, for β_0, β_1, $\lambda_{f,b,0}$, $\lambda_{f,b,1}$, and λ_z. To avoid ambiguity around pseudo-critical enthalpy, again, as with the temperature approximation, the parameters are chosen at least such that the thermal conductivity and the slope are continuous around pseudo-critical enthalpy. Slope and intercept of the linear part are chosen such that the linear approximation equals the experimental data through most of the low enthalpy region (NIST, 2013). This leaves one parameter open to discussion, which is the horizontal asymptote $\lambda_{f,b,1}$ of the exponential decay function. This is chosen as 0.7 times the minimum value for the thermal conductivity from the data.

β_0 = -3.2711 x_{10}^{-7} $Wm^{-1}K^{-1}J^{-1}kg$; β_1 = 1.3694 x_{10}^{-6} $kg\ J^{-1}$;

$\lambda_{f,b,0}$ = 1.0133 $Wm^{-1}K^{-1}$; $\lambda_{f,b,1}$ = 7.0154 x_{10}^{-2} $Wm^{-1}K^{-1}$; λ_z = 4.5553 $Wm^{-1}K^{-1}$.

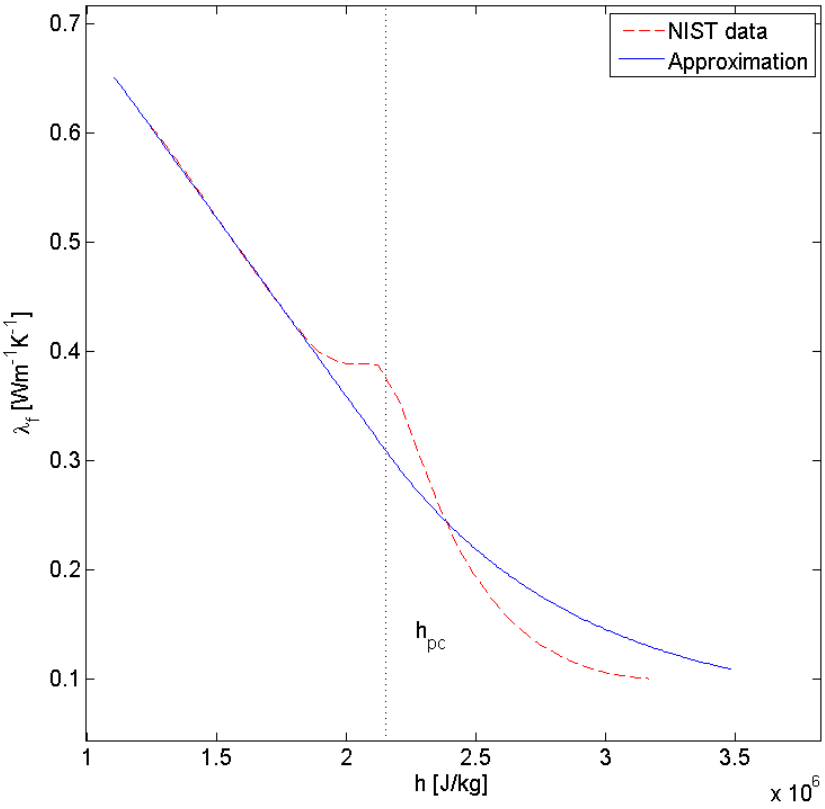

Figure 2.5. The thermal conductivity approximation from the equation of state. The red-dotted curve represents measurement data (NIST, 2013).

2.3. Transport balances

Krijger summarized the behaviour of the 4/5-node loop in a series of transport balance equations, governing mass, heat and momentum transport. Mass and heat transport were summarized for each node individually. The momentum balance was integrated along the entire loop. A few substitutions were applied, which resulted in a system of as many equations as there are unknown variables, which is uniquely solvable. The original balances of Krijger´s thesis are summarized in Appendix A of this thesis.

2.3.1. Low heating model

In Krijger's model the heat balance equation for the core (low heating model) reads:

$$AL\frac{d}{dt}\rho_0 H_0 = W_0 H_{IN} - W_{out} H_{out} + Q \tag{2.4}$$

The heat balance results from the constant heat Q and from the enthalpy-carrying mass flows $W_0 H_{IN}$, into the core section, and $W_{out} H_{out}$, flowing out. In the new model the heating Q is no longer directly fed to the coolant, so the Q term should be replaced with a term that accounts for the heat transfer from the wall to the channel. Such heat flux is written in the form:

$$q'' = -\alpha(T_0 - T_w) \tag{2.5}$$

in which the minus sign denotes that the heat flux occurs in the direction opposed to that of the temperature gradient. The factor α is the heat transfer coefficient and is one of the constituents of the Nusselt number *Nu*:

$$\alpha = \frac{Nu\lambda_f}{D_H} \tag{2.6}$$

Here D_H is the hydraulic diameter, which is 4 times the flow cross-sectional area A over the wetted perimeter P_{in} (van den Akker & Mudde, 1996). The assumption is made that the heat flux is homogeneous over the contact surface between the fluid and the wall. The total heat flow then becomes just the flux times the contact area $P_{in}L$.

$$q = \frac{Nu\lambda_f P_{in} L}{D_H}(T_w - T_0) \tag{2.7}$$

Now still an expression is needed for the Nusselt number *Nu*. Schenderling (2013), in his thesis, uses the model by Bishop et al. (1964):

$$Nu = 0.0069 Re^{0.9} Pr^{0.66} \left(\frac{\rho(H_w)}{\rho(H_0)}\right)^{0.43} \left(1 + 2.4\frac{D}{x}\right) \tag{2.8}$$

The factor $\left(1 + 2.4\frac{D}{x}\right)$ accounts for entrance region effects (Schenderling, 2013), which are not taken into account in this thesis. Therefore the factor is dropped, reducing the Nusselt number to:

$$Nu = 0.0069 Re^{0.9} Pr^{0.66} \left(\frac{\rho(H_w)}{\rho(H_0)}\right)^{0.43} \tag{2.9}$$

Re is the Reynolds number, for which an expression has already been set up in Krijger's (2013) thesis.

$$Re = \frac{W D_H}{A\mu} \tag{2.10}$$

The fraction $\rho(H_w)/\rho(H_0)$ in equation (2.9) accounts for the density difference between the fluid at bulk temperature and at wall temperature. *Pr* is the Prandtl number, which depends on the coolant thermal conductivity, as well as on the specific heat, which, as mentioned in section 2.2., is the inverse enthalpy-derivative of the temperature.

$$Pr = \frac{\mu c_p}{\lambda_f} = \frac{\mu}{\lambda_{f(H)}\frac{dT}{dH}} \tag{2.11}$$

The resulting heat balance reads:

$$\underline{\text{E0:}} \qquad \boldsymbol{AL\frac{d}{dt}\rho_0 H_0 = W_0 H_{in} - W_{out} H_{out} + \frac{Nu_0\lambda_{f,0}}{D_H} P_{in} L(T_w - T_0)} \tag{2.12}$$

The bold expression is used to emphasize that this equation is one of the governing balance equations of the system. The underscored 'E0' is used to indicate that this is the energy ('E') balance equation of node 0 ('0').

A heat balance for the wall is also required. With the assumption of temperature-independent heat capacity $c_{p,w}$ of the wall, the heat balance includes the wall cross-sectional area A_w, the wall density ρ_{wall} and the wall length L. The balance is constituted by the constant and homogeneous heating Q and the transfer term developed for the E0 balance equation above, but with a minus sign, as the heat flows out of the wall. The heat balance for the wall node therefore reads:

$$\underline{\text{Ew:}} \qquad \boldsymbol{\rho_w c_{p,w} A_w L\frac{d}{dt}T_w = Q - \frac{Nu_0\lambda_f}{D_H} P_{in} L(T_w - T_0)} \tag{2.13}$$

2.3.2. High heating model

In Krijger's thesis the heat balances for the core nodes read:

E0: $$A\rho_0 H_0 \frac{d}{dt} L_0 = W_0 H_{in} - W_{pc} h_{pc} + Q \frac{L_0}{L} \quad (2.14)$$

E1: $$A \frac{d}{dt} \rho_1 L_1 H_1 = W_{pc} h_{pc} - W_1 H_1 + Q \frac{L_1}{L} \quad (2.15)$$

The final term means that the magnitude of heating of the core nodes is proportional to their lengths. The same considerations as for the low heating model are applied, which result in the following equations:

E0: $$\boldsymbol{A\rho_0 H_0 \frac{d}{dt} L_0 = W_0 H_{in} - W_{pc} h_{pc} + \frac{Nu_0 \lambda_f}{D_H} P_{in} L_0 (T_{w,0} - T_0)} \quad \textbf{(2.16)}$$

E1: $$\boldsymbol{A \frac{d}{dt} \rho_1 L_1 H_1 = W_{pc} h_{pc} - W_1 H_1 + \frac{Nu_1 \lambda_f}{D_H} P_{in} L_1 (T_{w,1} - T_1)} \quad \textbf{(2.17)}$$

The heat balances for the wall nodes are similar to the one in the low heating model. The relevant terms include the heating Q proportional to the node lengths and the Nusselt-number dependent terms that account for the heat flows between the wall nodes and their respective core nodes. An additional term is needed in the balances, though, that accounts for the interaction between the wall nodes. This heat exchange occurs through conduction and the corresponding term should therefore be of the form:

$$q = q'' A_w = -\lambda_w \nabla T A_w \quad (2.18)$$

In which λ_w is the (assumed constant) thermal conductivity of the wall. The temperature gradient is written as follows:

$$\nabla T = \frac{\Delta T}{\Delta z} \quad (2.19)$$

In which a value needs to be appointed to the distance Δz between the wall nodes. For the sake of simplicity this is chosen as $L/2$, resulting in the following expression for the temperature gradient:

$$\nabla T = \frac{2\Delta T}{\mathrm{L}} \quad (2.20)$$

The term for the heat exchange among the wall nodes, $\frac{2\lambda_w}{L} A_w (T_{w,1} - T_{w,0})$, is added to the heat balances of the wall nodes. Their heat balances now read:

Ew0: $$\boldsymbol{\rho_w c_{p,w} A_w \frac{d}{dt} L_0 T_{w,0} = Q \frac{L_0}{L} - \frac{Nu_0 \lambda_f}{D_H} P_{in} L_0 (T_{w,0} - T_0) + \frac{2\lambda_w}{L} A_w (T_{w,1} - T_{w,0})} \quad \textbf{(2.21)}$$

Ew1: $$\boldsymbol{\rho_w c_{p,w} A_w \frac{d}{dt} L_1 T_{w,1} = Q \frac{L_1}{L} - \frac{Nu_1 \lambda_f}{D_H} P_{in} L_1 (T_{w,1} - T_1) - \frac{2\lambda_w}{L} A_w (T_{w,1} - T_{w,0})} \quad \textbf{(2.22)}$$

This system can be simplified a bit more. It is obvious that $L_0 + L_1 = L$ and as the time derivative of this relation is $\frac{dL_0}{dt} + \frac{dL_1}{dt} = 0$, it is visible that the E0 and E1 equations **(2.16)** and **(2.17)** can be unified to a single core fluid heat balance and the variable L_0 can be eliminated:

E1: $$\boldsymbol{(\rho_1 H_1 - \rho_0 H_0) A \frac{d}{dt} L_1 + A L_1 \frac{d}{dt} \rho_1 H_1 = W_0 H_{in} - W_1 H_1 \ldots}$$

$$\boldsymbol{\ldots + \frac{Nu_0 \lambda_f}{D_H} P_{in} (1 - L_1)(T_{w,0} - T_0) + \frac{Nu_1 \lambda_f}{D_H} P_{in} L_1 (T_{w,1} - T_1)} \quad \textbf{(2.23)}$$

Along with the balances M0, M1, MR, MB, ER, and I derived by Krijger and shown in Appendix A.2., these balances summarize the behaviour of the supercritical water loop model. Some of these balance equations have been omitted or substituted by Krijger. Also note that equation **(2.23)** *replaces* the existing heat balance for the channel core section, rather than being an addition to it. The same applies for the low-heating model, albeit the balances being given in Appendix A.1, rather than A.2.

2.4. Dimensionless balance equations and the adjusted Nusselt number

2.4.1. Dimensionless variables

In Krijger's thesis the transport balances are made dimensionless, in order to construct dimensionless parameters that describe the operation conditions of the system, which in turn makes it easier to examine the behaviour of different configurations compared to each other. Steady state variables for the parameter X will be denoted as $\overline{X}$, and perturbations as $\breve{x}$. An underlined variable $\underline{X}$ means that the variable is dimensionless.

The dimensionless variables are summarized in Table 2.1.

Table 2.1. Overview of the dimensionless variables. All variables in the left column are adopted from Krijger's (2013) thesis.

$\underline{\overline{L}_i} = \frac{\overline{L}_i}{L}$	Length, steady state	$\underline{T_i} = \left(\frac{\lambda_{f,pc} L}{Q}\right) T_i$	Temperature
$\underline{\breve{l}_i} = \frac{\breve{l}_i}{L}$	Length, perturbation	$\underline{\breve{\theta}_i} = \left(\frac{\lambda_{f,pc} L}{Q}\right) \breve{\theta}_i$	Temperature, perturbation
$\underline{t} = \frac{t\overline{W} v_{pc}}{LA}$	Time	$\underline{\alpha_i} = \left(\frac{Q \lambda_{f,pc} L}{\overline{W}^2}\right) \alpha_i$	Quadratic temperature approximation coefficient
$\underline{\overline{W}_i} = \frac{\overline{W}_i}{\overline{W}} = 1$	Mass flow, steady state	$\underline{c_{p,i}} = \frac{\overline{W} c_{p,i}}{\lambda_{f,pc} L}$	Specific heat capacity
$\underline{\breve{w}_i} = \frac{\breve{w}_i}{\overline{W}}$	Mass flow, perturbation	$\underline{P_{in}} = \frac{P_{in}}{L}$	Contact perimeter between channel and wall
$\underline{\overline{H}_i} = \frac{\overline{H}_i \overline{W}}{Q}$	Specific enthalpy, steady state	$\underline{\lambda_w} = \frac{\lambda_w A}{\lambda_{f,pc} L^2}$	Wall thermal conductivity
$\underline{\breve{h}_i} = \frac{\breve{h}_i \overline{W}}{Q}$	Specific enthalpy, perturbation	$\underline{A_w} = \frac{A_w}{A}$	Wall cross-sectional area
$\underline{\overline{\rho}_i} = \overline{\rho}_i v_{pc}$	Density, steady state	$\underline{\lambda_f} = \frac{\lambda_f}{\lambda_{f,pc}}$	Coolant fluid thermal conductivity
$\underline{\breve{\rho}_i} = \breve{\rho}_i v_{pc}$	Density, perturbation	$\underline{\beta_0} = \frac{\beta_0 Q}{\lambda_{f,pc} \overline{W}}$	Coolant thermal conductivity linear approximation coefficient
$\underline{D_H} = \frac{D_H}{L}$	Hydraulic diameter	$\underline{\beta_1} = \beta_1 \frac{Q}{\overline{W}}$	Coolant thermal conductivity exponential approximation coefficient
$\underline{\overline{V}_B} = \frac{\overline{V}_B}{AL}$	Buffer vessel volume, steady state		

2.4.2. Adjusted Nusselt number

The dimensionless equations given in the next subsections 2.4.3. and 2.4.4. will be linearized in the subsequent section 2.5. For convenience in linearization, the specific enthalpy-dependent coolant thermal conductivity λ_f is isolated from the rest of the Nusselt number, leaving a multiplication factor considered unperturbed, which we will call the adjusted Nusselt number.

$$\widehat{Nu} = Nu\lambda_f^{0.66} \tag{2.24}$$

This means that a commonly found factor in this thesis, $Nu\lambda_f$, must be replaced using the relation $Nu\lambda_f = \widehat{Nu}\lambda_f^{0.34}$. Note that the adjusted Nusselt number is no longer dimensionless, so for dimensionless linear analysis also its dimensionless version needs to be introduced.

$$\underline{\widehat{Nu}_0} = \frac{\widehat{Nu_0}}{\lambda_{f,pc}^{0.66}} \tag{2.25}$$

2.4.3. Low heating model

In this subsection the dimensionless heat balance equations of the channel core section and the core wall for the low-heating model are given. The remaining dimensionless balance equations of the system do not differ from those posed by Krijger. These equations are given in Appendix A.3.

The variable W_{out} can be substituted by using the explicit expression $W_{out} = AL_R\frac{d}{dt}\rho_R + W_R$, following from the physical MR mass balance (See Appendix A.1.) (Krijger, 2013). The temperature T_0, through use of equation (2.2) is substituted by the quadratic approximation, which means that the temperature difference $T_w - T_0$ becomes $T_w - T_0 = T_w - \alpha_0\left(H_0 - h_{pc}\right)^2 - \frac{1}{c_{p,pc}}\left(H_0 - h_{pc}\right) - T_{pc}$. Substituting these relations into the energy balances and making the latter dimensionless yields the following equations:

E0: $$\underline{\frac{d}{dt}\boldsymbol{\rho_0 H_0}} = \underline{\boldsymbol{W_0 H_{in}}} - \underline{\boldsymbol{H_{out}}}\left(\underline{\boldsymbol{L_R}}\,\underline{\frac{d}{dt}\boldsymbol{\rho_R}} + \underline{\boldsymbol{W_R}}\right)\ldots$$

$$\ldots + \underline{\widehat{\boldsymbol{Nu_0}}}\,\underline{\boldsymbol{\lambda_{f0}^{0.34}}}\,\underline{\frac{\boldsymbol{P_{in}}}{\boldsymbol{D_H}}}\left(\underline{\boldsymbol{T_w}} - \underline{\boldsymbol{T_{pc}}} - \underline{\boldsymbol{\alpha_0}}\left(\underline{\boldsymbol{H_0}} - \underline{\boldsymbol{h_{pc}}}\right)^2 - \underline{\frac{1}{\boldsymbol{c_{p,pc}}}}\left(\underline{\boldsymbol{H_0}} - \underline{\boldsymbol{h_{pc}}}\right)\right) \tag{2.26}$$

Ew: $$\underline{\boldsymbol{\rho_w c_{p,w} A_w}}\,\underline{\frac{d}{dt}\boldsymbol{T_w}} = \boldsymbol{1} - \underline{\widehat{\boldsymbol{Nu_0}}}\,\underline{\boldsymbol{\lambda_{f0}^{0.34}}}\,\underline{\frac{\boldsymbol{P_{in}}}{\boldsymbol{D_H}}}\left(\underline{\boldsymbol{T_w}} - \underline{\boldsymbol{T_{pc}}} - \underline{\boldsymbol{\alpha_0}}\left(\underline{\boldsymbol{H_0}} - \underline{\boldsymbol{h_{pc}}}\right)^2 - \underline{\frac{1}{\boldsymbol{c_{p,pc}}}}\left(\underline{\boldsymbol{H_0}} - \underline{\boldsymbol{h_{pc}}}\right)\right) \tag{2.27}$$

2.4.4. High heating model

Applying the same operations of substituting and making dimensionless as done in previous subsection, the following dimensionless energy balances for the high-heating model are obtained:

E1: $$\underline{\boldsymbol{L_1}}\,\underline{\frac{d}{dt}\boldsymbol{\rho_1 H_1}} + \left(\underline{\boldsymbol{\rho_1 H_1}} - \underline{\boldsymbol{\rho_0 H_0}}\right)\underline{\frac{d}{dt}\boldsymbol{L_1}} = \underline{\boldsymbol{W_0 H_{in}}} - \underline{\boldsymbol{W_1 H_1}}\ldots$$

$$\ldots + \underline{\widehat{\boldsymbol{Nu_0}}}\,\underline{\boldsymbol{\lambda_{f0}^{0.34}}}\,\underline{\frac{\boldsymbol{P_{in}}\left(\boldsymbol{1}-\underline{\boldsymbol{L_1}}\right)}{\boldsymbol{D_H}}}\left(\underline{\boldsymbol{T_{w,0}}} - \underline{\boldsymbol{T_{pc}}} - \underline{\boldsymbol{\alpha_0}}\left(\underline{\boldsymbol{H_0}} - \underline{\boldsymbol{h_{pc}}}\right)^2 - \underline{\frac{1}{\boldsymbol{c_{p,pc}}}}\left(\underline{\boldsymbol{H_0}} - \underline{\boldsymbol{h_{pc}}}\right)\right)$$

$$\ldots + \underline{\widehat{\boldsymbol{Nu_1}}}\,\underline{\boldsymbol{\lambda_{f1}^{0.34}}}\,\underline{\frac{\boldsymbol{P_{in}}\boldsymbol{L_1}}{\boldsymbol{D_H}}}\left(\underline{\boldsymbol{T_{w,1}}} - \underline{\boldsymbol{T_{pc}}} - \underline{\boldsymbol{\alpha_1}}\left(\underline{\boldsymbol{H_1}} - \underline{\boldsymbol{h_{pc}}}\right)^2 - \underline{\frac{1}{\boldsymbol{c_{p,pc}}}}\left(\underline{\boldsymbol{H_1}} - \underline{\boldsymbol{h_{pc}}}\right)\right) \tag{2.28}$$

Ew0: $$\underline{\rho_w}\underline{c_{p,w}}\underline{A_w}\left(\mathbf{1}-\underline{L_1}\right)\frac{d}{d\underline{t}}\underline{T_{w,0}}-\underline{\rho_w}\underline{c_{p,w}}\underline{A_w}\underline{T_{w,0}}\frac{d}{d\underline{t}}\underline{L_1}=\mathbf{1}-\underline{L_1}\ \ldots$$

$$\ldots-\underline{\widehat{Nu_0}}\underline{\lambda_{f0}^{0.34}}\frac{\underline{P_{in}}\left(1-\underline{L_1}\right)}{\underline{D_H}}\left(\underline{T_{w,0}}-\underline{T_{pc}}-\underline{\alpha_0}\left(\underline{H_0}-\underline{h_{pc}}\right)^2-\frac{1}{\underline{c_{p,pc}}}\left(\underline{H_0}-\underline{h_{pc}}\right)\right)\ldots$$

$$\ldots+2\underline{\lambda_w}\underline{A_w}\left(\underline{T_{w,1}}-\underline{T_{w,0}}\right) \qquad \textbf{(2.29)}$$

Ew1: $$\underline{\rho_w}\underline{c_{p,w}}\underline{A_w}\underline{T_{w,1}}\frac{d}{d\underline{t}}\underline{L_1}+\underline{\rho_w}\underline{c_{p,w}}\underline{A_w}\underline{L_1}\frac{d}{d\underline{t}}\underline{T_{w,1}}=\underline{L_1}\ \ldots$$

$$\ldots-\underline{\widehat{Nu_1}}\underline{\lambda_{f1}^{0.34}}\frac{\underline{P_{in}}\underline{L_1}}{\underline{D_H}}\left(\underline{T_{w,1}}-\underline{T_{pc}}-\underline{\alpha_1}\left(\underline{H_1}-\underline{h_{pc}}\right)^2-\frac{1}{\underline{c_{p,pc}}}\left(\underline{H_1}-\underline{h_{pc}}\right)\right)\ldots$$

$$\ldots-2\underline{\lambda_w}\underline{A_w}\left(\underline{T_{w,1}}-\underline{T_{w,0}}\right) \qquad \textbf{(2.30)}$$

The remaining dimensionless equations, again, do not differ from those posed by Krijger (See Appendix A.4.).

2.5. Linearized transport balances

2.5.1. Linearization

In order to reduce the system of differential equations to a linear system, all time dependent variables are linearized. Without going too much into detail on this procedure, the most important steps are explained here. The linearization is done by writing every non-constant variable X as a sum of its steady state value and a perturbation, resulting in $X=\overline{X}+\breve{x}$. Subsequently, as some terms in the equations have more than one time dependent factor – suppose they'd be of the form $X_1X_2=\left(\overline{X}_1+\breve{x}_1\right)\left(\overline{X}_2+\breve{x}_2\right)$ – non-linear perturbation terms still exist. But considering that an introduced perturbation is small compared to a steady state value, it will not strike one as surprising that the multiplication of two perturbations will be even smaller. Therefore, in the outcome, the term $\breve{x}_1\breve{x}_2$ will be neglected. The same applies for terms of the form $\breve{x}_1\frac{d}{dt}\breve{x}_2$. What will be left is a set of equations that are sums of the steady state dimensionless equations described in the previous section and perturbation terms that are linear in the perturbed variables. The steady state terms are subtracted from both sides of the equations and a set of *n* first order linear differential equations with *n* variables remain.

The linearization of the properties modelled through the equation of state (section 2.2.) is done with a first order Taylor expansion, as higher order terms are multiplications of perturbations and can be neglected. For example, as fluid temperature is a function of specific enthalpy alone, the perturbation in fluid temperature can be written as $\underline{\breve{\theta}}=\left.\frac{d\underline{T}}{d\underline{H}}\right|_{H=\overline{H}}\underline{\breve{h}}=\left(2\underline{\alpha_i}\left(\underline{H_i}-\underline{h_{pc}}\right)+\frac{1}{\underline{c_{p,pc}}}\right)\underline{\breve{h}}$, provided that both $T(H)$ and $\frac{dT}{dH}$ are continuous over the whole *H* domain. The same can be done for the fluid thermal conductivity. In the equation of state approximation of the specific volume a slope discontinuity occurs at $H=h_{pc}$ (Krijger, 2013). The dependence of the Nusselt number on the Prandtl number and the density fraction is not taken into account.

The linearized energy balances of the channel core section and the core wall for the low-heating model and high-heating model will be given in the subsections 2.5.2. and 2.5.3. respectively. As with the physical and dimensionless balances, the linearized balances posed by Krijger for the low- and high-heating models are given in Appendix A.5. and A.6. respectively.

2.5.2. Low heating model

The linearized heat balances for the low heating model are:

E0: $$\left(\frac{1}{2}\overline{\rho_0}+\frac{1}{2}C_1N_{\Delta h}h_{pc}v_{pc}\overline{H_0}\right)\frac{d}{dt}\breve{h}_{out}+C_1N_{\Delta h}h_{pc}v_{pc}\overline{H_{out}}L_R\frac{d}{dt}\breve{h}_R=\cdots$$

$$\ldots-\breve{w}_R\overline{H_{out}}+\breve{w}_0\overline{H_{in}}+\widehat{Nu_0}\bar{\lambda}_{f0}^{0.34}\frac{P_{in}}{D_H}\breve{\theta}_w\ldots$$

$$\ldots-\left(\widehat{Nu_0}\frac{P_{in}}{D_H}\left(\left(\alpha_0\left(H_0-h_{pc}\right)+\frac{1}{2c_{p,pc}}\right)\bar{\lambda}_{f0}^{0.34}-0,17\bar{\lambda}_{f0}^{-0.66}\left(\overline{T_w}-\overline{T_0}\right)\beta_0\right)+1\right)\breve{h}_{out}\quad\textbf{(2.31)}$$

Ew: $$\rho_w c_{p,w}A_w\frac{d}{dt}\breve{\theta}_w=-\widehat{Nu_0}\bar{\lambda}_{f0}^{0.34}\frac{P_{in}}{D_H}\breve{\theta}_w\ldots$$

$$\ldots+\frac{1}{2}\widehat{Nu_0}\frac{P_{in}}{D_H}\left(\bar{\lambda}_{f0}^{0.34}\left(2\alpha_0\left(H_0-h_{pc}\right)+\frac{1}{c_{p,pc}}\right)-0,34\bar{\lambda}_{f0}^{-0.66}\left(\overline{T_w}-\overline{T_0}\right)\beta_0\right)\breve{h}_{out}\quad\textbf{(2.32)}$$

2.5.3. High heating model

For the high heating model the linearized equations read:

E1: $$\frac{\overline{L_1}}{\overline{v_1}}\left(1-\frac{N_{\Delta h}C_1h_{pc}\overline{H_1}}{v_{pc}\overline{v_1}}\right)\frac{d}{dt}\breve{h}_1+\left(\frac{\overline{H_1}}{\overline{v_1}}-H_0\rho_0\right)\frac{d}{dt}\breve{L}_1=H_{in}\breve{w}_0-\overline{H_1}\breve{w}_1+\widehat{Nu_0}\overline{\lambda_{f0}^{0.34}}\frac{P_{in}\overline{L_0}}{D_H}\widetilde{\theta_{w,0}}\ldots$$

$$\ldots-\left(\widehat{Nu_1}\frac{P_{in}\overline{L_1}}{D_H}\left(\left(2\alpha_1\left(H_1-h_{pc}\right)+\frac{1}{c_{p,pc}}\right)\overline{\lambda_{f1}^{0.34}}+0,34\left(\overline{T_{w,1}}-\overline{T_1}\right)\overline{\lambda_{f1}^{-0,66}}\beta_1\lambda_z e^{-\beta_1\overline{H_1}}\right)+1\right)\widetilde{h_1}\ldots$$

$$\ldots+\widehat{Nu_1}\overline{\lambda_{f1}^{0.34}}\frac{P_{in}\overline{L_1}}{D_H}\widetilde{\theta_{w,1}}+\frac{P_{in}}{D_H}\left(\widehat{Nu_1}\overline{\lambda_{f1}^{0.34}}\left(\overline{T_{w,1}}-\overline{T_1}\right)-\widehat{Nu_0}\overline{\lambda_{f0}^{0.34}}\left(\overline{T_{w,0}}-T_0\right)\right)\breve{L}_1\quad\textbf{(2.33)}$$

Ew0: $$\rho_w c_{p,w}A_w\overline{L_0}\frac{d}{dt}\widetilde{\theta_{w,0}}-\rho_w c_{p,w}A_w\overline{T_{w,0}}\frac{d}{dt}\breve{L}_1=\left(\widehat{Nu_0}\overline{\lambda_{f0}^{0.34}}\frac{P_{in}}{D_H}\left(\overline{T_{w,0}}-T_0\right)-1\right)\breve{L}_1\ldots$$

$$\ldots-\left(\widehat{Nu_0}\overline{\lambda_{f0}^{0.34}}\frac{P_{in}\overline{L_0}}{D_H}+2\lambda_w A_w\right)\widetilde{\theta_{w,0}}+2\lambda_w A_w\widetilde{\theta_{w,1}}\quad\textbf{(2.34)}$$

Ew1: $$\rho_w c_{p,w}A_w\overline{T_{w,1}}\frac{d}{dt}\breve{L}_1+\rho_w c_{p,w}A_w\overline{L_1}\frac{d}{dt}\widetilde{\theta_{w,1}}=\left(1-\widehat{Nu_1}\overline{\lambda_{f1}^{0.34}}\frac{P_{in}}{D_H}\left(\overline{T_{w,1}}-\overline{T_1}\right)\right)\breve{L}_1\ldots$$

$$\ldots+\widehat{Nu_1}\frac{P_{in}\overline{L_1}}{D_H}\left(\left(2\alpha_1\left(\overline{H_1}-h_{pc}\right)+\frac{1}{c_{p,pc}}\right)\overline{\lambda_{f1}^{0.34}}+0,34\left(\overline{T_{w,1}}-\overline{T_1}\right)\overline{\lambda_{f1}^{-0,66}}\beta_1\lambda_z e^{-\beta_1\overline{H_1}}\right)\widetilde{h_1}\ldots$$

$$\ldots+2\lambda_w A_w\widetilde{\theta_{w,0}}-\left(\widehat{Nu_1}\overline{\lambda_{f1}^{0.34}}\frac{P_{in}\overline{L_1}}{D_H}+2\lambda_w A_w\right)\widetilde{\theta_{w,1}}\quad\textbf{(2.35)}$$

2.6. Stability characteristics

2.6.1. Dimensionless numbers

Typically the operating conditions in a LWR are summarized by two dimensionless numbers, one being a measure for the heating power and the other for the inlet enthalpy. Krijger (2013) adopted measures that were slightly modified from the ones used by T'Joen & Rohde (2012). These measures are used again in this thesis and in subsection 2.6.2. their convenience will become apparent.

$$N_{sub} = 1 - \frac{H_{IN}}{h_{pc}} \tag{2.36}$$

$$N_{\Delta h} = \frac{Q}{\overline{W} h_{pc}} \tag{2.37}$$

N_{sub} is the sub-cooling number, a measure for the inlet specific enthalpy. The sub-cooling number *decreases* with increasing enthalpy. It is assumed that the inlet enthalpy will not exceed the pseudo-critical enthalpy at any time during operation, although there is no physical mechanism that prevents it from doing so. Furthermore, as negative enthalpy is unphysical, the sub-cooling number cannot exceed 1.

$N_{\Delta h}$ is the pseudo phase change number, and is a measure for the enthalpy increase in the core section. In contrast to the situation in forced systems, where the mass flow W is "dictated" by pumps, here the mass flow attains a value as a consequence of the heating power Q.

2.6.2. Steady state solutions

In steady state operation, all time derivative terms are zero. Parameter values at steady state result from the operating conditions and geometry. For every point in the operating plane (the plane containing every operating conditions ($N_{\Delta h}$, N_{sub})) a steady state situation can be determined. The steady state parameter values will be needed to perform the eventual stability analysis at that operating point. From every balance equation (from the physical transport balances discussed in section 2.3., not the linearized ones) follows a steady state value for the time-dependent variable governed. In the low heating model the steady state solutions are:

$$\overline{H_0} = H_{in} + \frac{Nu_0 \lambda_f P_{in} L (\overline{T_w} - \overline{T_0})}{2 \overline{W} D_H} \tag{2.38}$$

$$\overline{T_w} = \frac{Q D_H}{Nu_0 \lambda_f P_{in} L} + \overline{T_0} \tag{2.39}$$

Note that these solutions are interdependent. One may attempt to find independent analytical solutions based on the equation of state approximations, but, as will be shown further on, in the numerical finding of these solutions, the interdependent descriptions will suffice.

The steady state solutions to the balance equations for the high heating model are:

$$\overline{L_0} = \frac{D_H \overline{W} (h_{pc} - H_{in})}{Nu_0 \lambda_f P_{in} (\overline{T_{w,0}} - \overline{T_0})} = \frac{D_H \overline{W} h_{pc} N_{sub}}{Nu_0 \lambda_f P_{in} (\overline{T_{w,0}} - \overline{T_0})} \tag{2.40}$$

$$\overline{H_1} = h_{pc} + \frac{Nu_1 \lambda_f P_{in} \overline{L_1}}{D_H \overline{W}} \left(\overline{T_{w,1}} - \overline{T_1} \right) \tag{2.41}$$

$$\overline{T_{w,0}} = \frac{Q\frac{\overline{L_0}}{L} + \frac{Nu_0 \lambda_f P_{in} \overline{L_0}}{D_H}\overline{T_0} + \frac{2\lambda_w}{L} A_w \overline{T_{w,1}}}{\frac{Nu_0 \lambda_f P_{in} \overline{L_0}}{D_H} + \frac{2\lambda_w}{L} A_w} \tag{2.42}$$

$$\overline{T_{w,1}} = \frac{Q\frac{\overline{L_1}}{L} + \frac{Nu_1 \lambda_f P_{in} \overline{L_1}}{D_H}\overline{T_1} + \frac{2\lambda_w}{L} A_w \overline{T_{w,0}}}{\frac{Nu_1 \lambda_f P_{in} \overline{L_1}}{D_H} + \frac{2\lambda_w}{L} A_w} \tag{2.43}$$

The length L_0 may equal or exceed the total core length L according to equation (2.40), but this is inconsistent with the use of the high heating model. If $L_0 = L$, then it must hold that $L_1 = 0$. Consequently it can be shown using the equations (2.40) through (2.43) that $N_{\Delta h} = N_{sub}$. This condition is represented by a line in the plane of operational conditions. Left of the line, where $N_{\Delta h}$ is smaller than N_{sub}, the low heating model applies, and to the right, where $N_{\Delta h}$ exceeds N_{sub}, the high heating model holds.

2.6.3. Transient behaviour

The time evolution of the system can be presented as a matrix-vector system of the form:

$$A\frac{d}{dt}\vec{x} = B\vec{x} \tag{2.44}$$

In which A and B are coefficient matrices for the time derivatives of the variables and the variables themselves respectively. The coefficient matrices for this problem are given in Appendix B. In the low heating model they are 5x5 matrices (5 linearized transport balances times 5 time-dependent variables, each element accounting for one variable in one equation) and in the high heating model their sizes are 8x8. The matrices represent the coefficients of the linearized transport balances from subsection 2.5..

The vector $\vec{x}$ contains the perturbed variables x_k. The solution for this matrix-vector system is of the form $\vec{x} = \sum_{i=1}^{n} c_i \vec{v}_i e^{\lambda_i t}$, where $\vec{v_i}$ is the i-th eigenvector of some governing matrix M, whose components describe the amplitude and phase shift of the i-th contribution to the perturbation with index i at $t=0$. The i-th eigenvalue $\lambda_i = r_i + j\omega_i$ (not to be confused with the thermal conductivity) of matrix M, consists of a real and an imaginary part. The number of terms of the solution n is the number of perturbed variables (either 5 or 8, depending on whether the low or high heating model is applied) and c_i is some summation coefficient that depends on the condition of the system at $t=0$.

For a stability investigation, only the eigenvalues λ_i are of interest. If the real part of an eigenvalue r_i is negative, then its exponential $e^{\lambda_i t}$ will become smaller than unity and its contribution to the perturbation $\vec{x}$ will die out over time ($DR < 1$). If this is the case for all contributions $e^{\lambda_i t}$ in the system, then the system is considered stable. If one of the eigenvalues has a real part that is positive, then at least one of the perturbed variables will diverge ($DR > 1$) , dragging other variables with it and destabilizing the system. Therefore such a situation is unstable.

The imaginary part of an eigenvalue ω_i is the angular frequency of an oscillation associated with the i-th contribution to the perturbation. Several of these oscillations will occur at the same time, but eventually the oscillation with the largest amplitude – the largest positive r_m – will come to dominate. The imaginary part ω_m of the eigenvalue λ_m is then the resonance frequency of the destabilized system.

3. COMPUTATIONAL IMPLEMENTATION

3.1. Considerations

The computational implementation is done by modification of a MATLAB code that has been developed by Krijger (2013). During scripting, Krijger paid specific attention to the readability of the code. Other considerations kept in mind were flexibility for input parameters. While computational speed was regarded an important factor as well, it had not been emphasized as much, due to the simplicity of the calculations (Krijger, 2013).

The modifications applied to the code account for the core wall thermal inertia in the system. Various input parameters are implemented, that describe properties of the wall, such as thermal conductivity, specific heat capacity and cross sectional area. The set of iterative steady state calculations and definitions for dimensionless variables are expanded and the coefficient matrices are extended to include the linearized heat balances of the wall nodes.

In the low heating model, if the input parameter describing the wall cross-sectional area is set to zero, then the left side of the heat balance of the wall, equation (2.13), becomes zero. Substituting this equation in equation (2.12) reduces the latter to equation (2.4), the heat balance of the core section of the channel in the Krijger (2013) case. Similar reasoning can be applied to the high heating model, using equations (2.21), (2.22) and (2.23). It can be concluded that the limit case with an infinitely small wall cross-sectional area, ceteris paribus, equals the Krijger case. This is used as a benchmark.

Other points of attention include the channel core enthalpy never exceeding pseudo-critical enthalpy in the low heating model, the length of node 1 being equal to or larger than zero in the high heating model and the steady state mass flow being real valued. Violations of these requirements are listed in the MATLAB command window after the computational job is finished.

Technical details on the algorithm are discussed in the following section.

3.2. Algorithm

3.2.1. Structure

The algorithm follows the structure of Krijger's code. At the start of the code the whole of MATLAB workspace, figures, etc. is cleaned up. From there on, about 30 input parameters are specified. These parameters describe geometry (e.g. hydraulic diameter), fluid properties (e.g. the parameters describing the equation of state), the domain of the instability map and computational performance. With the latter properties such as the resolution *NxN* of the instability map are meant, as well as the accuracy of the iteration process for acquiring steady state values, which will be discussed more thoroughly in section 3.2.2.. In general this means a trade-off between computational speed and performance, as higher resolution and accuracy require more calculations. A visualization of the algorithm structure is presented in Figure 3.1. The code itself is supplied in Appendix D.1.

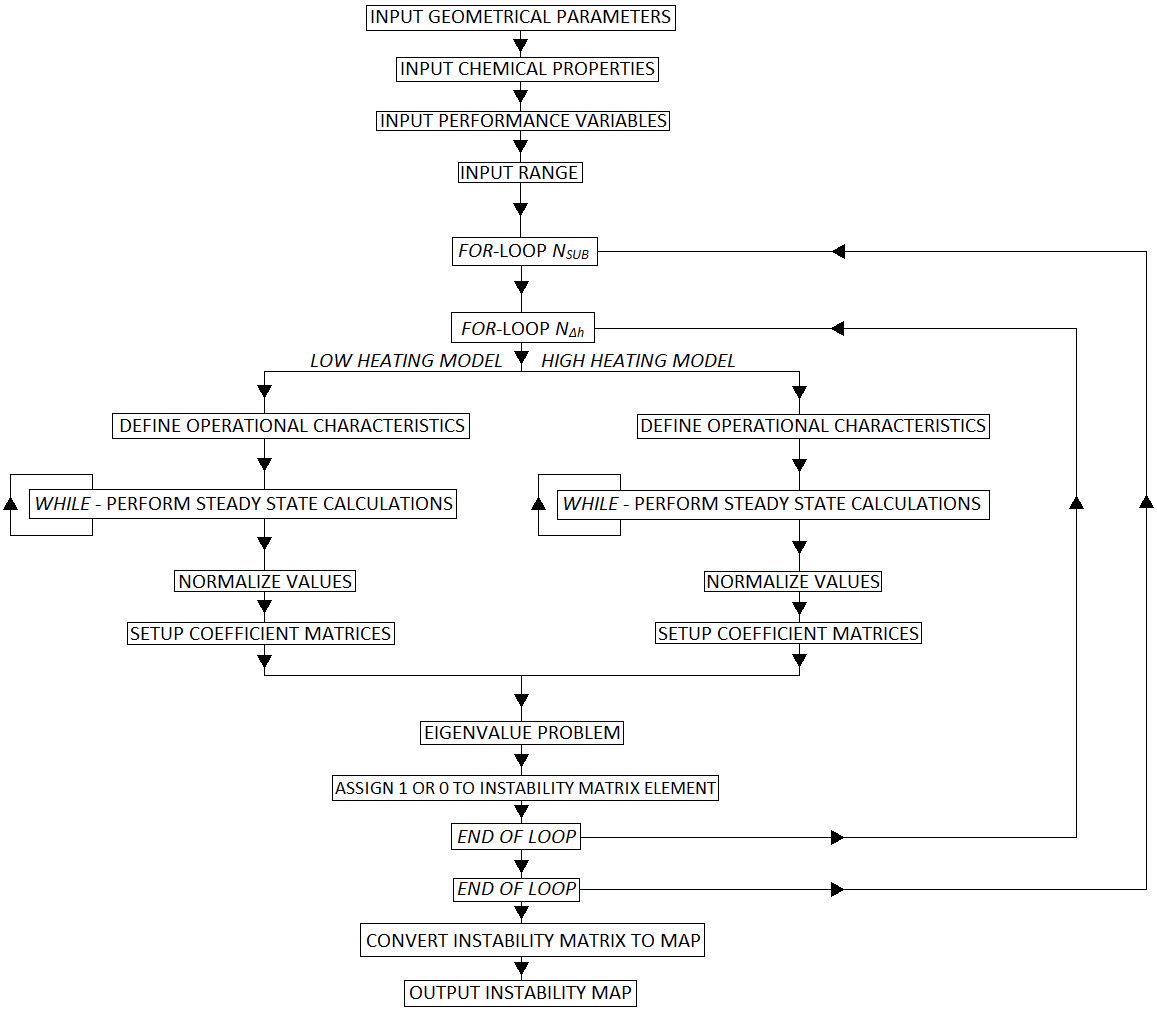

Figure 3.1. General structure of the algorithm for generating instability maps.

After specification of the input parameters, the code enters a double *for*-loop, that concerns every point in the plane of operational conditions N_{sub} and $N_{\Delta h}$ within the specified limits. Initially in the loop, operational characteristics (such as inlet enthalpy) that are flow-independent are formulated. Subsequently, through iteration, the steady state flow values are calculated. These values are normalized (i.e. made dimensionless) and the coefficient matrices for the eigenvalue problem are formulated. Thus, for every point on the map the eigenvalue problem is solved. Next it is determined whether the set of eigenvalues complies to the stability requirement. For every point on the map exists an element in an *NxN* matrix that describes whether the system is stable at the operational conditions in that point.

Finally, the matrix is converted to a colour map, in which unstable regions are highlighted in red and stable regions are coloured blue. Additional modifications can be made so that the output also displays Ledinegg instabilities and resonance frequencies. A parametric study on the behaviour of the NSB can also be implemented.

3.2.2. Acquiring steady state values

Specific attention needs to be paid to the calculation of the steady state values. In Krijger's code, with exception of the mass flow rate and the Reynolds number, all operational characteristics, such as steady-state values for several enthalpies and the lengths of the nodes describing the channel core sections in the high-heating model, are defined directly, i.e. without the use of iterative calculations. In this system the operational characteristics cannot be expressed explicitly. The initial estimations required for the iteration process equal the explicit expressions of Krijger's code, but the characteristics are re-evaluated in the *while*-loop calculating the steady state flow, this time taking into account the interdependencies between the steady state values, as described in subsection 2.6.2.

In Krijger's code the accuracy of iterative calculations is such that the loop of calculations stops when the relative difference in mass flow between the two last iterations $(W_i - W_{i-1})/W_{i-1}$ is smaller than $w_{res}=10^{-12}$. In the new code an input command for w_{res} is included at the input section of the code, so that the user can decide on a trade-off between the accuracy of the calculations and computational speed, for example when running a test case.

Several functions are used for the implementation of the equation of state for specific volume, temperature and coolant thermal conductivity. These functions are named SPECVOL, TMPR and THERMC respectively. The functions require an input parameter H describing the specific enthalpy in the node considered and yield an output value v, T, or λ_f describing specific volume, temperature and coolant thermal conductivity respectively. A converse function named ENTH requires an input temperature T and yields an output enthalpy H. These functions employ the equations (2.1), (2.2), (2.3a) and (2.3b) as well as the general formula for solving second-order polynomial equations (ENTH). The MATLAB codes of these functions are shown in Appendices D.2. through D.5..

3.2.3. Eigenvalue problem, instability matrix and instability map

The time dependent matrix-vector equation (2.44) is solved using the EIG function in MATLAB. The EIG function uses QZ factorisation to solve a generalised eigenvalue problem, which is needed because the coefficient matrix A is singular, and therefore A^{-1}, which is needed for solving the normal eigenvalue problem, does not exist (Krijger, 2013). The solution to the generalised eigenvalue problem for n x n matrices may include less than n eigenvalues. However, for reasons unclear, MATLAB always returns exactly n values, some of which are not eigenvalues (Koren, 2010). They are typically very large numbers, usually infinite. These values are disregarded in the dynamic stability analysis, by setting an upper limit to the magnitudes of the values regarded.

Right after the input section of the code the instability matrix is initialized to be an NxN matrix MAT of zeroes. If the stability criterion is met for conditions $N_{sub} = N_{sub,i}$ and $N_{\Delta h} = N_{\Delta h,k}$, then the matrix element $MAT_{i,k}$ will be designated the value 1. The remaining elements of MAT retain the value zero. Finally, this matrix of zeroes and ones is finally converted into a map of red and blue areas denoting dynamically unstable and stable regions respectively.

3.2.4. Modifications

Krijger has also included several modifications to the code which allow for more specific investigation of the stability behaviour. The modifications are listed below:

- Parametric study: In order to investigate the influence of a specific input parameter on the neutral stability boundary, neutral stability boundaries are plotted in a single figure for specified values of the specified input parameter. The neutral stability boundary is computed from the *MAT* matrix, by finding every element with value 1 that has at least one neighbouring 0.

- Resonance frequency study: For all dynamically unstable points the imaginary parts of the eigenvalues are also investigated. The resonance frequency is given by the frequency of the eigenvalue with the largest positive real part. Different frequencies are displayed by different colours on the instability map. Dynamically unstable regions with zero frequency are, however, not distinguishable from dynamically stable regions in these figures, so a resonance frequency study figure alone cannot provide complete information on the dynamic stability of the specified system.

- Ledinegg instability map: Studying the mass flow rate versus power characteristics for different sub-cooling numbers, Krijger (2013) found that Ledinegg instabilities can occur for a given sub-cooling number, if the slope of the characteristic swaps signs at least three times (See Figure 3.2). This definition is used to determine whether a point is situated within a Ledinegg unstable region. Ledinegg unstable points may coincide with dynamically stable points and statically stable points may conversely coincide with dynamically unstable points.

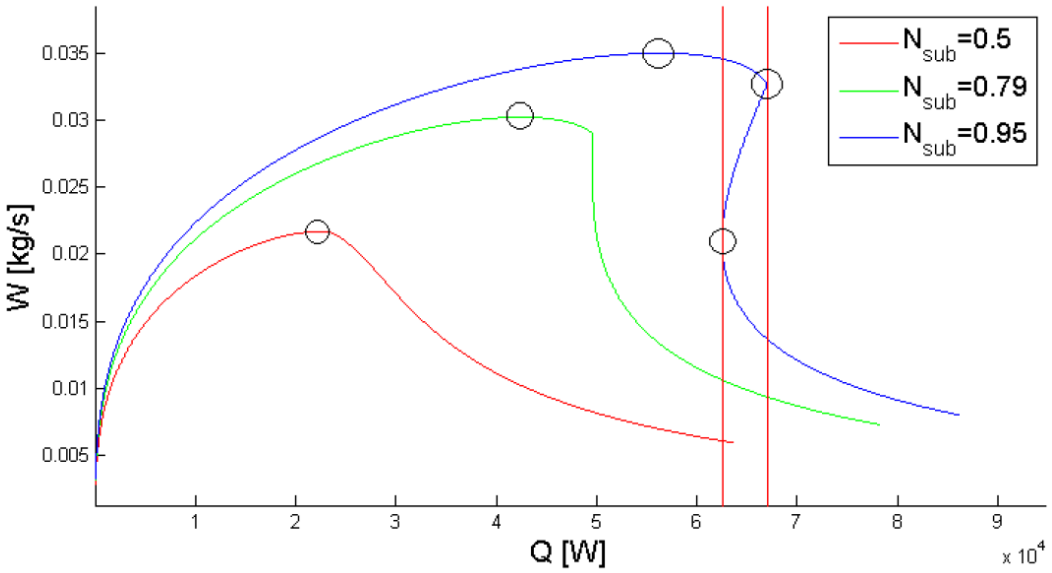

Figure 3.2. Mass flow rate versus power characteristics for several sub-cooling numbers. The Ledinegg unstable region for N_{sub}=0.95 is bordered by the vertical red lines. The black circles indicate sign swaps in the slopes of the mass flow rate versus power characteristics (Krijger, 2013).

4. RESULTS

4.1. Reference case

In this chapter several results will be presented and compared to those from a reference case. The reference case was initially set up by Krijger (2013) and has been extended in this thesis. Numerical values of the input parameters on which the reference case is based are supplied in Appendix C. These values closely resemble corresponding geometrical parameters of the HPLWR, for example the core section channel length of 4.2 m (Ortega Gómez, 2009). The wall cross-sectional area for the reference case was chosen as equal to the channel cross-sectional area, as the qualitative behaviour of the neutral stability boundary was expected to be mainly a matter of the order of magnitude of the wall cross-section, rather than a matter of a factor 0.5 or 2. Figure 4.1. shows the dynamic instability map resulting from the input parameters as specified in this reference case.

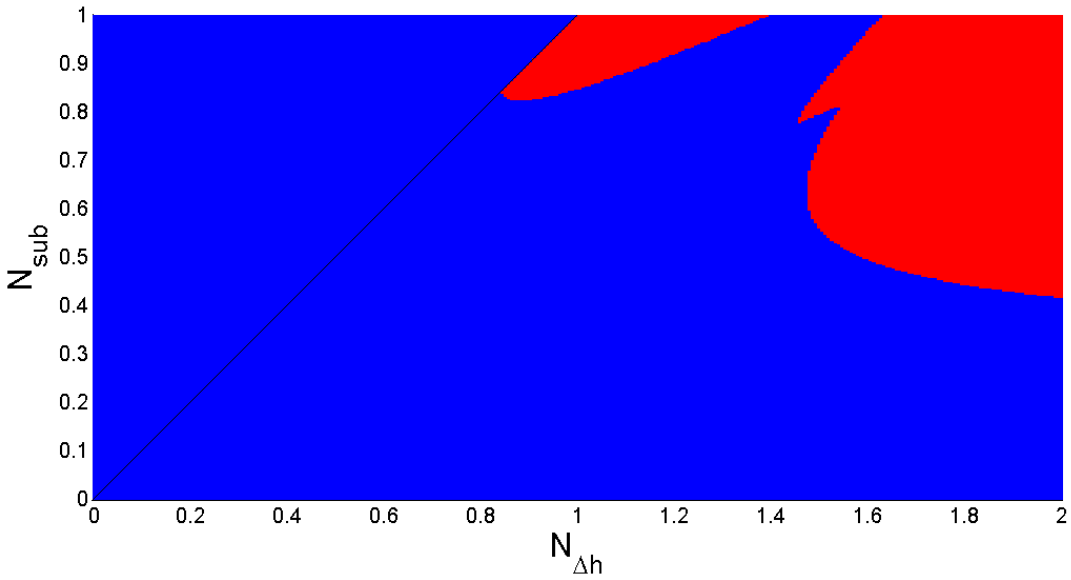

Figure 4.1. Instability map for the reference case.

The line $N_{sub} = N_{\Delta h}$ shows the range of operational conditions where pseudocritical enthalpy is reached in the top of the core. The NSB characteristic right of the line $N_{sub} = N_{\Delta h}$ in the high subcooling region shows similarities to the NSB found by T'Joen & Rohde (2012), but lies in a much higher subcooling region. This may be a result of the simplicity of this model, as well as the difference in geometry between this model and the DeLight experimental setup. Differences in thermodynamic properties between water and Freon R23 may also play a role.

For comparison, the situation in which the wall cross-section is assumed zero is shown in Figure 4.2, where it is overlaid with the neutral stability boundary of the Krijger (2013) reference case. Since the stability boundaries match, the benchmark posed in section 3.1. is complied to. It is visible that the presence of the wall has a stabilizing effect and a right-upward trend, as is found by Schenderling (2013), is visible as well. The stabilizing effect that wall thermal inertia displays is further investigated in the next section.

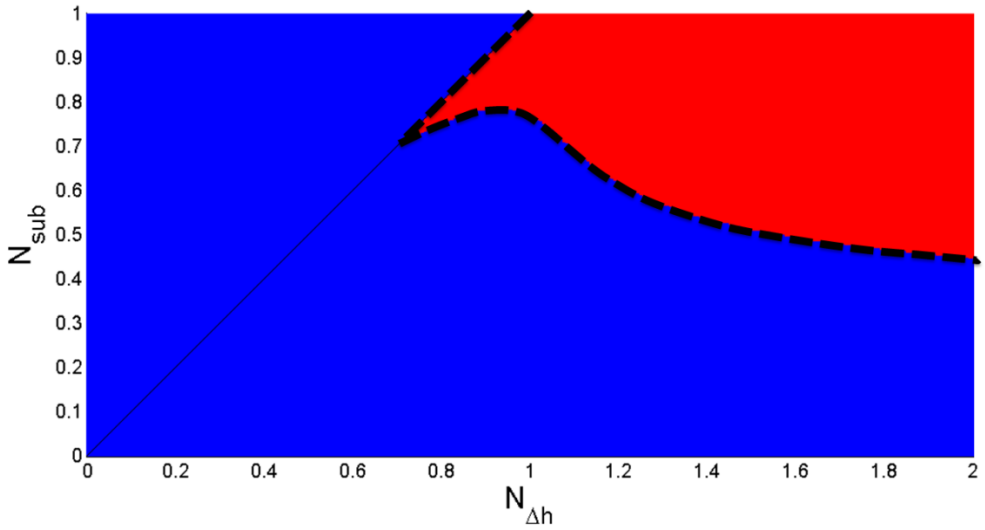

Figure 4.2. Instability map in the limit case of an infinitely small wall cross-sectional area $A_w=0$. The dashed curve is the neutral stability boundary from the reference case by Krijger (2013).

4.2. Parametric study

4.2.1. Wall cross-sectional area

A ceteris paribus parametric study is performed on the influence of the cross-sectional area of the core wall on the behaviour of the Neutral Stability Boundary.

The first study considers the wall cross section smaller than the channel flow area. The heat influx from the power source Q is, in contrast to the zero-wall cross-section case, no longer equal to the Nusselt-dependent radial heat transfer term plus the axial conduction term – from the balance equations Ew, Ew0 and Ew1 can be seen that the wall nodes' temperatures negatively correlate with their time derivatives (e.g. an increase in $T_{w,1}$ leads to a decrease in $d(T_{w,1})/dt$). These negative feedback mechanisms are expected to have a stabilising effect, when considered individually.

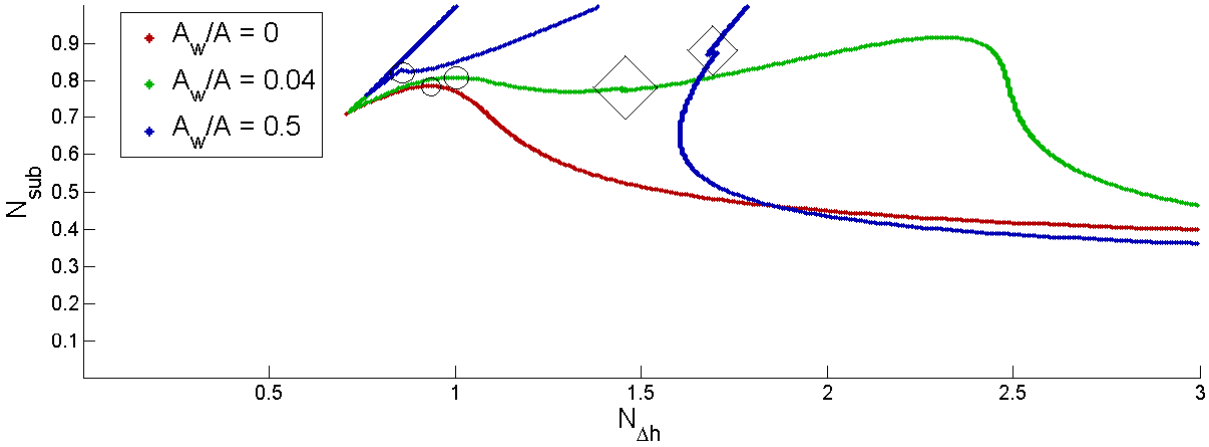

Figure 4.3. Neutral stability boundaries for small wall cross-sectional areas. The circles highlight local maxima of N_{sub} vs $N_{\Delta h}$.

Inclusion of the wall, in comparison to the zero-cross-section limit case, shows that the expected stabilising effect is of a significant magnitude, as shown by the increase of the area under the neutral

stability boundaries in Figure 4.3. As the wall cross-section grows though, the stability declines in the high pseudo phase change region.

Judged from the general trends in each of the curves, it seems plausible that the encircled N_{sub}-local maxima in the NSB's are each other's counterparts. As will become clear in the investigation of larger wall cross-section cases (Figure 4.5), these bumps "dissolve" in the $N_{sub} = N_{\Delta h}$ line,

The NSB's for the cases A_w/A=0.04 and A_w/A=0.5 both show another, smaller, bump, highlighted in Figure 4.3 by diamonds. These bumps may have a common cause as well, which will be further investigated in the larger wall cross-section cases.

The decline of the stability in the high pseudo phase change region with increasing wall cross-sections continues through cases of wall cross-sections that are in the same order of magnitude as the channel flow area, as is shown in Figure 4.4.

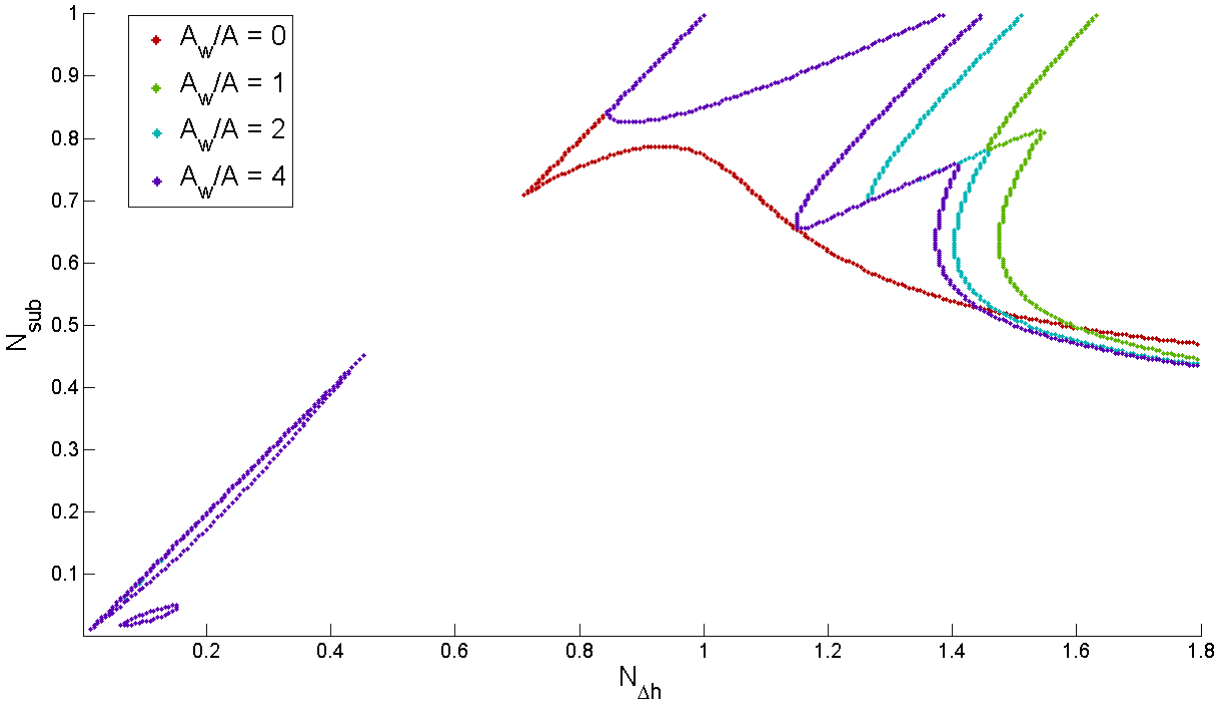

Figure 4.4. Neutral stability boundaries for cross-sections in the range of the channel flow area. The zero wall cross-section limit case is plotted in red as a reference.

The small bumps that were highlighted with diamonds in Figure 4.3 show more significance in these cases (that is of course, under the assumption that they are the same bumps). They appear to divide the unstable region in the top right of the instability map into multiple regions.

Also note that previously unseen unstable regions originate in the low sub-cooling and low pseudo phase change region, starting around A_w/A=2. The regions appear just under the $N_{\Delta h}=N_{sub}$ line. A study on the resonance frequencies is performed, in an attempt to find a cause to attribute these phenomena to. The A_w/A=4 case is studied and the frequency map is displayed in Figure 4.5.

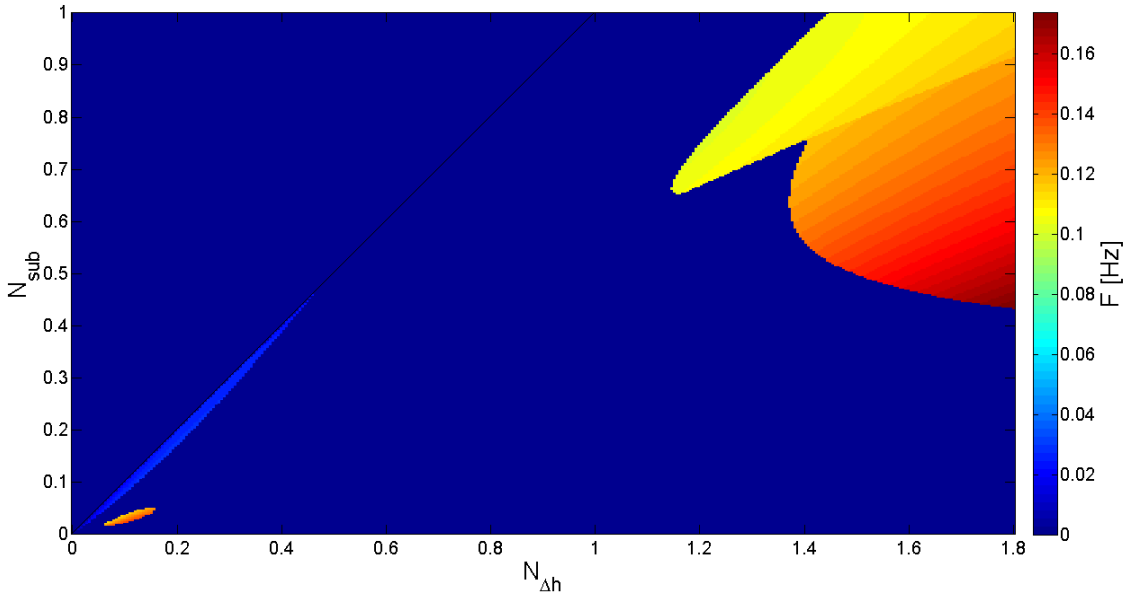

Figure 4.5. Resonance frequencies for A_w/A=4.

We can roughly divide these instabilities into five regions, as is done in Figure 4.6. Region I, in the high subcooling region, mid-range pseudo phase change, is invisible on the frequency map, but can clearly be seen in Figure 4.4. It indicates that this instability region shows no oscillatory behaviour. Regio II, the dark blue region in the bottom left, has low-range resonance frequencies of about 0.04 Hz, possibly associated with a long residence time, which can be expected from an instability resulting from an interaction between the core and the riser. Region III contains higher resonance frequencies, typically around 0.13 Hz, suggesting a more core-driven instability. Regions IV and V are adjacent to each other and the distinction is somewhat vague, as in the border region the two instability regimens seem to conflict. The border can roughly be represented by a line from the edge (the "diamond-highlighted bump") near ($N_{\Delta h}$=1.4, N_{sub}=0.7) to the upper right corner of the figure. Interestingly, the stability boundaries for all cases in Figure 4.4 run partially along that border.

Finally we investigate the behaviour of a wall that has a much larger cross section than the channel flow area. In the hypothetical case of an infinitely large wall, as the heat balance $\rho_w c_{p,w} A_w L \frac{d}{dt} T_w$ is expected to be finite, the temperature of the wall must be constant over time. The results are shown in Figure 4.6. In the regions IV and V the stability boundary stays more or less the same for bigger wall cross-sections and in region I it does not change at all. Region II (not to be confused with type II instabilities) shrinks slightly as region III slightly expands.

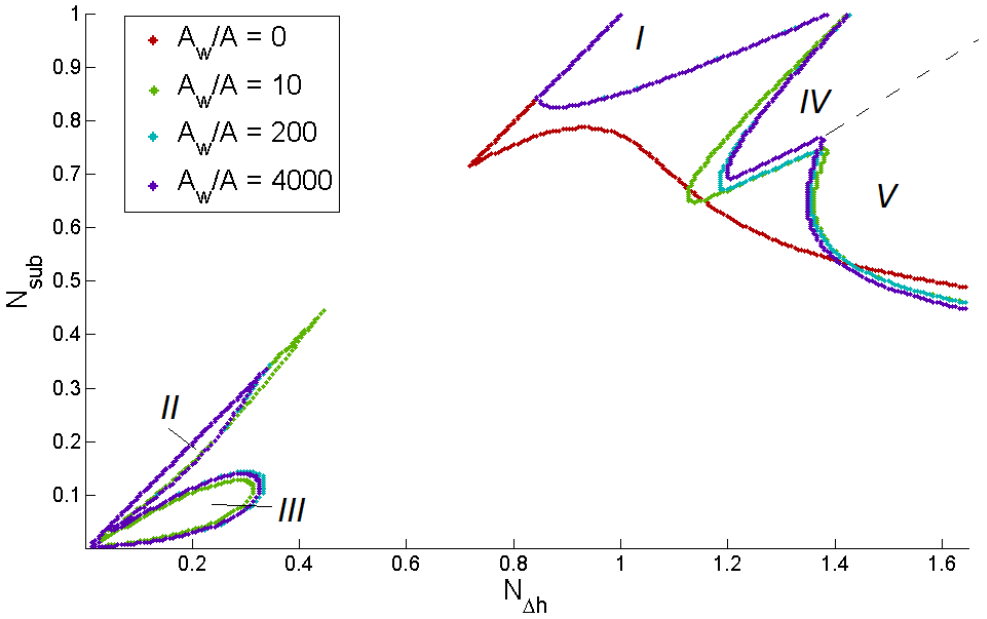

Figure 4.6. Neutral stability boundaries for large wall cross-sections. The zero wall cross-section limit case is plotted in red as a reference.

To find out how the resonance regimens change with growing wall cross-sections, a final frequency study is performed in the limit case where A_w/A=4000. This value is chosen as a limit due to a computational limitation, i.e. the iterative steady state calculations (discussed in subsection 3.2.2.) cease to converge around A_w/A=4000. From Figure 4.7 it seems that the instabilities in region II do not show oscillatory behaviour. The resonance frequencies in region III have significantly dropped as well, from around 0.13 Hz in the A_w/A=4 case to about 0.08 Hz. The distinction between regions IV and V has become clearer in comparison to the A_w/A=4 case, as the whole of region IV oscillates at almost the same frequency, around 0.10 Hz.

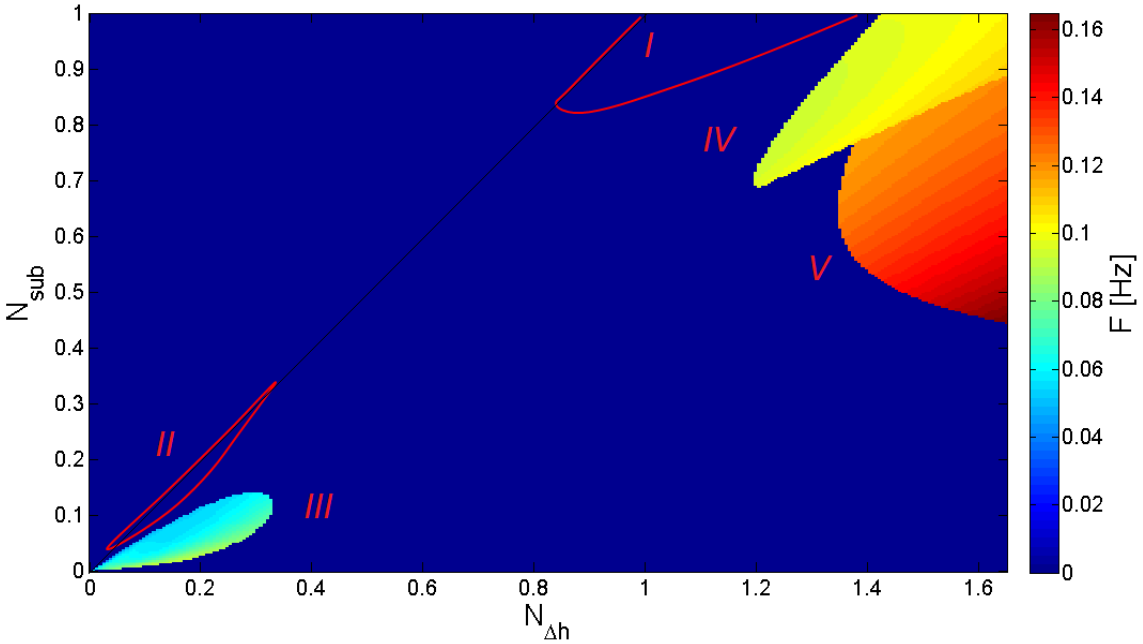

Figure 4.7. Resonance frequencies for the limit case A_w/A=4000.

4.2.2. Wall thermal conductivity

We want to see the influence of the interaction between the wall nodes as well. This can be done by performing a parametric study on the thermal conductivity of the wall nodes λ_w.

The behaviour is studied for two wall cross-sections, one being equal to the channel flow area, the other being thirty-five times that. The stability boundary is expected to be more sensitive to varying wall thermal conductivity at large wall cross-sections, as the terms in the heat balances Ew0 and Ew1, accounting for the heat conduction between the wall nodes, are linearly dependent on both A_w and λ_w. The choice for A_w/A=35 comes from the same computational restriction as the choice for A_w/A=4000 as the limit case in the study on the wall cross-sectional area, namely the iterative steady state calculations ceasing to converge. The results are displayed in Figure 4.8.

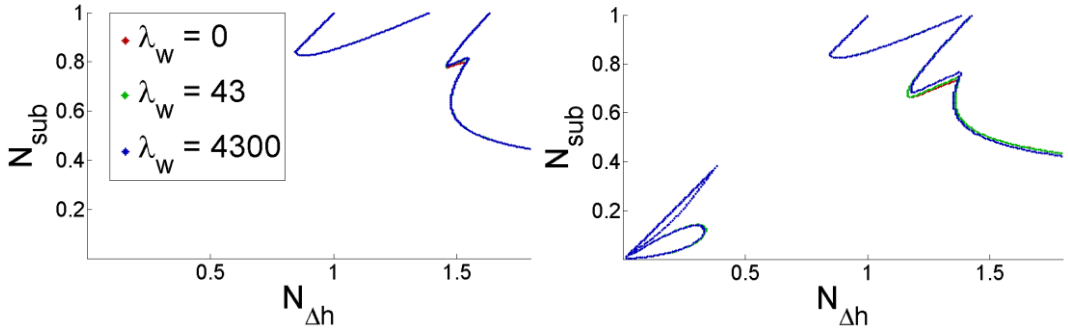

Figure 4.8. Parametric study on the effect of the wall thermal conductivity for A_w/A=1 (left) and A_w/A=35 (right). While the wall thermal conductivity has a bigger effect on the NSB when the wall cross-section is larger, the effect has generally little significance.

As is shown, the thermal conductivity of the walls is of almost no influence on the stability boundaries. A closer look at the heat balances Ew0 and Ew1 could have led us to expect this non-significance, as the value of the temperature difference weighing factor of the wall-to-channel heat transfer term $\frac{Nu_0\lambda_f}{D_H}P_{in}L_0$ is typically around 75 W K^{-1}, whereas that of the axial thermal conduction $\frac{2\lambda_w}{L}A_w$ is typically of the order 10^{-4} W K^{-1}. This suggests that the effect of axial thermal conduction is almost negligible in the heat balances, except at very high thermal conductivities.

A test case was conducted, studying a case with wall thermal conductivity λ_w=0 and cross-section A_w/A=10^{10} and all other parameters matching those of the reference case (see Appendix C). In the test case, no failure to converge arose in the iterative steady state calculations, whereas cases with finite wall thermal conductivity tend to run into trouble as the wall cross-sections get larger (such as the limit case A_w/A=4000 in subsection 4.2.1.). It seems that the convergence of the iterative calculations requires a condition specifying an upper limit to the contributions of thermal conduction between the wall nodes to the heat balances, for example $\frac{2\lambda_w}{L}A_w \ll \frac{Nu_0\lambda_f}{D_H}P_{in}L_0$.

It must be kept in mind that only axial thermal conduction was taken into account, as temperature was considered constant over a whole node, requiring radial thermal conductivity to be infinite in all cases.

4.2.3. Channel geometry

We expect the scaling of the channel to have, compared to the scaling of the wall cross-sectional area, a similar but reverse effect on the neutral stability boundary, as an increase in channel cross-section A means that the ratio A_w/A is reduced. A parametric study on the channel flow area is performed. It must be kept in mind that a change in channel flow area A affects other parameters of the channel geometry, such as the hydraulic diameter D_H and the wetted perimeter P_{in}, as well. Since in the most simple geometries $A \propto D^2$ in which D is some channel width – not necessarily the hydraulic diameter – the scaling of the hydraulic diameter by a factor r, so $D_{H,i} = rD_{H,ref}$, in which the subscript *ref* denotes the reference value, is complemented by the scaling of the channel flow area by a factor r^2, so $A_i = r^2 A_{ref}$. The wall cross section is kept constant at its reference value of 35.5 mm^2. This means that the ratio of the wall cross-section over the channel flow area A_w/A is scaled by $\frac{1}{r^2}$. In the momentum balance I (Appendix A.1., equation (A.6)) the upscaling of the hydraulic diameter exerts a positive influence on the correlation between the mass flows in the core and riser sections and their time derivatives. The heat balance Ew shows a similar effect on the correlation between the wall node temperature and its time derivative. From this an increase in hydraulic diameter is expected to destabilize the system. Krijger (2013) however found a destabilizing effect for a decrease in the hydraulic diameter, due to the outlet friction increasing more than the inlet friction because of a lower density in the riser. It must be noted that Krijger (2013) does not mention the simultaneous scaling of the channel flow area, which may exert another influence on the system, although from the balance equations it is unclear whether this effect will be stabilizing or destabilizing.

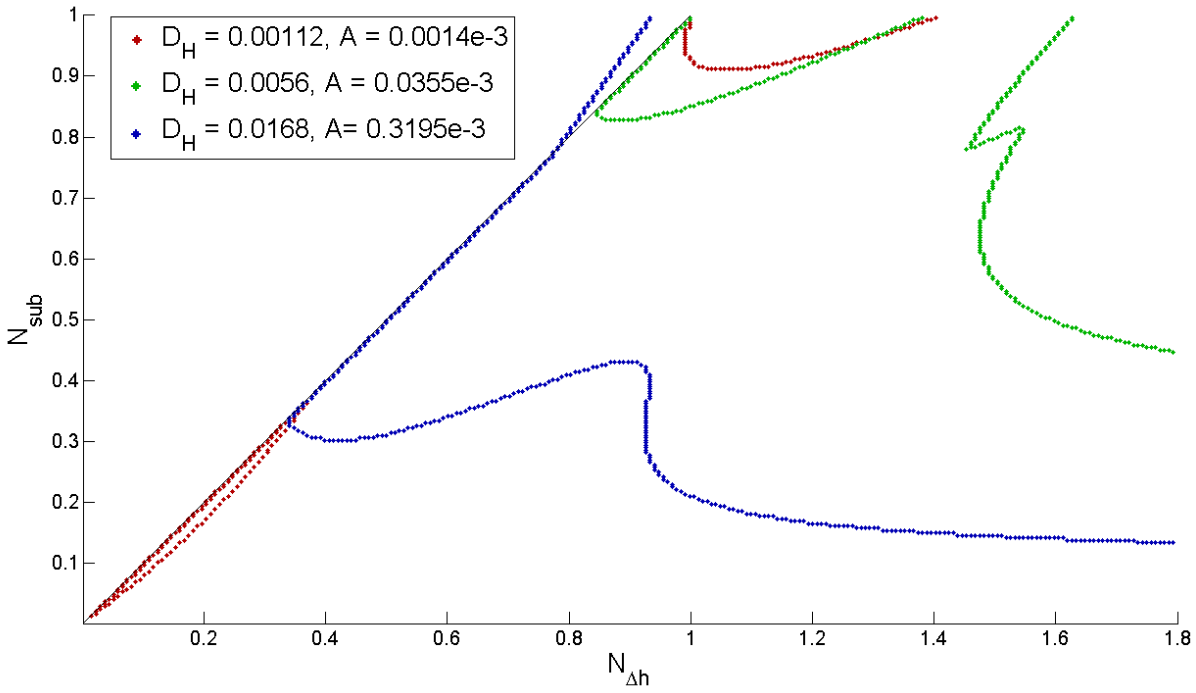

Figure 4.9. Parametric study on channel geometry. An unstable region emerges in the bottom left in the case of a downscaled channel, as shown by the red curve.

An unstable region emerges in the bottom left after downscaling the channel. From a frequency analysis we try to find out to which of the two newly found instability regions, II or III, this one corresponds. Some reference frequencies are needed to compare those in this region to. Since region

I consists of non-oscillating instabilities, we must turn to regions IV and V to find reference frequencies, so therefore we need a wider pseudo phase change range. The resulting frequency map is displayed in Figure 4.10 and it shows that this region probably corresponds to region II, as the resonance frequencies are in a very low range, compared to the frequencies in the upper right of Figure 4.10.

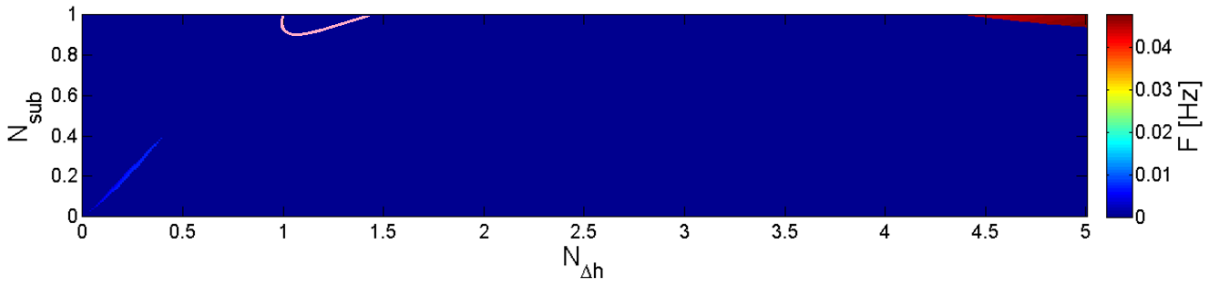

Figure 4.10. Resonance frequencies for the case D=1.12mm, A=1.42mm^2, A_w=35.5mm^2. In the bottom left corner is an instability region with a very low resonance frequency compared to the resonance frequencies associated with the instability in the upper right corner.

4.3. Ledinegg instability

Using Krijger's code for finding Ledinegg instabilities, one Ledinegg unstable region has been found near region I. The occurrence of Ledinegg instabilities is independent of the dynamic stability of the system. The Ledinegg map is computed for A_w/A=10 in order to find out whether the newly found regions, II and III, contain Ledinegg instabilities. The NSB of the dynamic instability map is laid over the Ledinegg instability map in Figure 4.11.

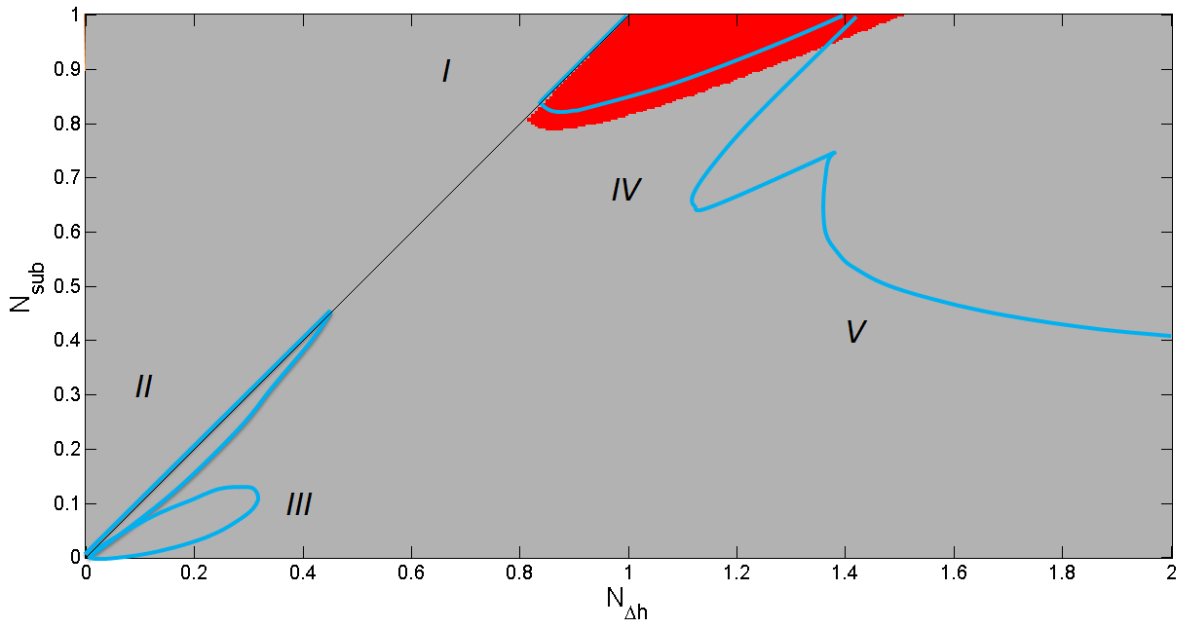

Figure 4.11. Map of the Ledinegg instability. The red region is the region where Ledinegg instabilities can occur. Plotted over the map is the dynamic neutral stability boundary (blue).

Figure 4.11 shows that the newly found regions, II and III, do not contain Ledinegg instabilities. The found Ledinegg instability region covers most of instability region I, part of region IV and part of the dynamically stable region between them.

An earlier look into the Krijger (2013) case showed a Ledinegg instability region that was similar to that of the above case. To study the similarity, the Ledinegg region (grey) of the Krijger case is laid over the Krijger case dynamic stability map. The Ledinegg instability boundary (yellow) of the above *Aw/A=10* case is then laid over the composite map of the Krijger case. The resulting image is displayed in Figure 4.12.

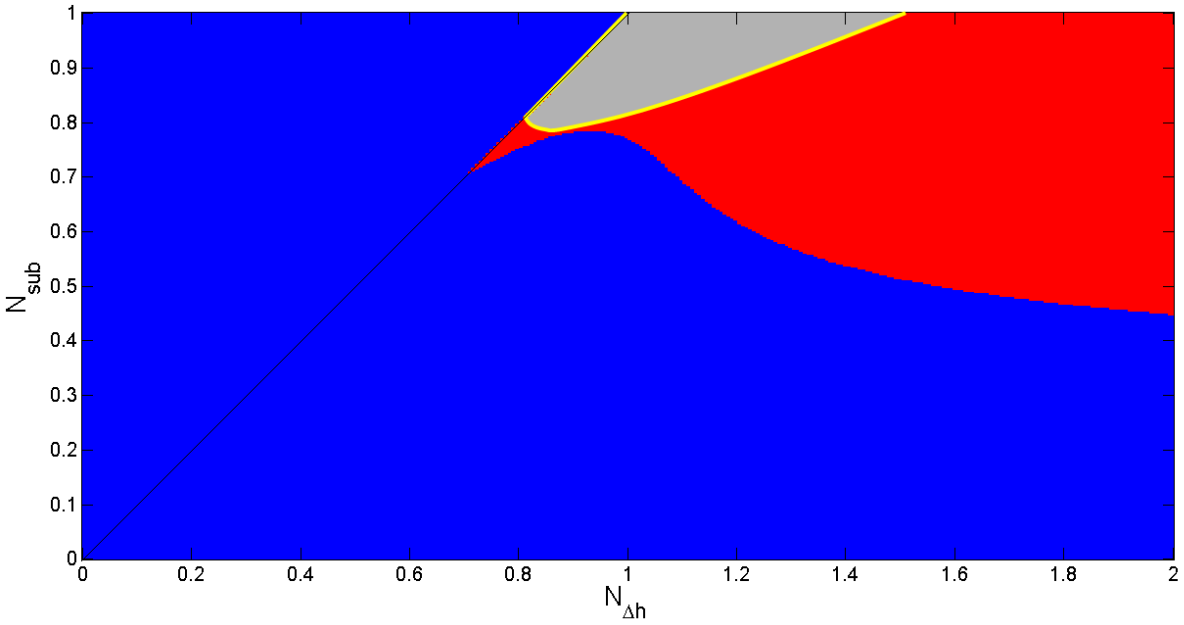

Figure 4.12. The Ledinegg instability region of the Krijger case (grey) laid over the dynamic stability map of the Krijger case (blue for stable, red for unstable) and topped with the Ledinegg instability boundary of the A_w/A=10 case (yellow).

It is found that the Ledinegg instability region of the A_w/A=10 case matches the Ledinegg instability region of the Krijger limit case. This is not so surprising, since the parameter A_w directly influences only two kinds of terms of the whole system of balance equations. On one hand there are the terms describing axial heat conduction between the wall nodes in the heat balances Ew0 and Ew1 – which are found in subsection 4.2.2. to be of very little significance – and on the other are the terms on the left side of the heat balances Ew, Ew0 and Ew1 of the wall nodes. The significance of A_w in the latter is diminished by the fact that A_w is multiplied by the time derivative of the temperature, which is zero by the definition of steady state. From this can be concluded that, as long as the influence of axial heat conduction between the wall nodes is very small, the Ledinegg instabilities are almost unaffected by the magnitude of the wall cross-section.

4.4. The variability of coolant thermal conductivity

Initially, in the research period, the thermal conductivity had been assumed constant. It was already halfway through the research period that a parametric study was performed on the influence of the thermal conductivity on the stability boundary. The effect was significant and therefore it was then decided to assume thermal conductivity as an enthalpy-dependent variable, as had been done earlier

for the specific volume and the temperature. Figure 4.13 shows the neutral stability boundaries for the case A_w/A=10 in which the coolant thermal conductivity is assumed to be enthalpy-dependent and a case in which it is assumed constant.

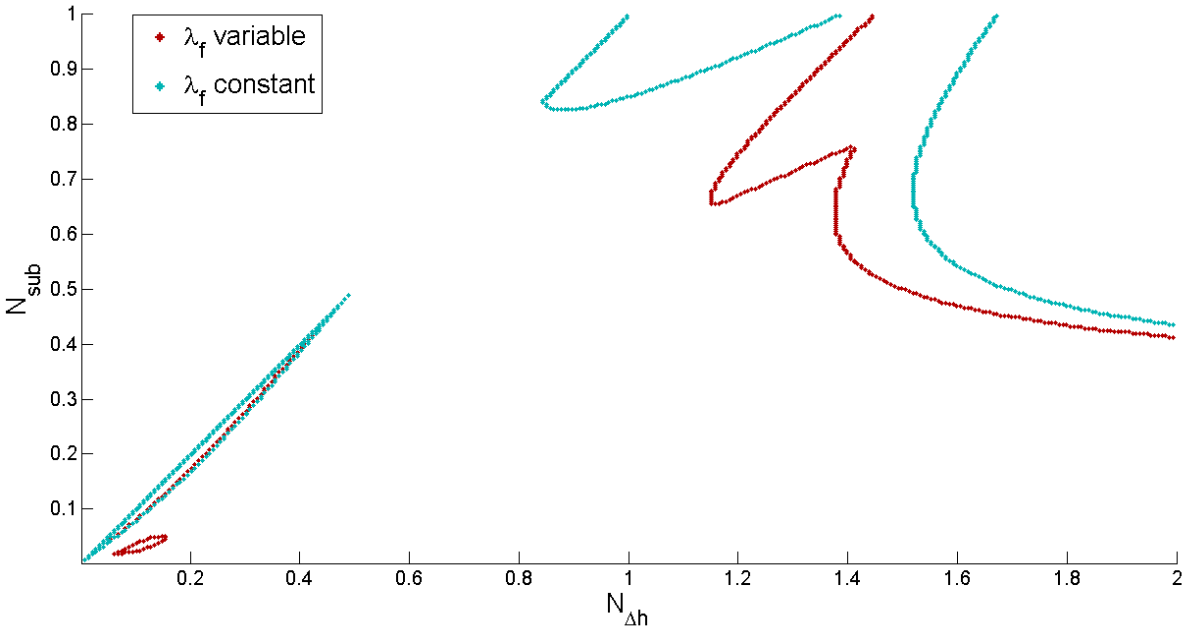

Figure 4.13. Neutral stability boundaries for the A_w/A=10 case, one with coolant thermal conductivity assumed constant (turquoise) and the other with coolant thermal conductivity assumed enthalpy-dependent (red).

The effect of the enthalpy-dependent coolant thermal conductivity is significant. The neutral stability boundary, which is shown to decline in the upper-right region as the wall cross-section is enlarged, shows a stronger decline in the enthalpy-dependent coolant thermal conductivity case than it does in the case where the coolant thermal conductivity is assumed constant. The constant coolant thermal conductivity case also shows no distinction between unstable regions IV and V (Figures 4.6 and 4.7) by the neutral stability boundary, nor does it contain the unstable region III.

The rightmost regions on the stability map have high heating power in the core section. This leads to generally higher temperatures, and thereby to lower coolant thermal conductivities in the enthalpy-dependent thermal conductivity model. As λ_f drops, then the factor $\lambda_f^{0.34}$ weighing the negative feedback – stabilizing – effect in the *dimensionless* heat balance E0 (equation (2.26)) drops as well. With this reasoning the difference in decline between the neutral stability boundaries in high pseudo phase change regions is not very surprising. Its significance however calls for further investigation of the several thermodynamic properties, such as coolant dynamic viscosity.

5. CONCLUSIONS AND RECOMMENDATIONS

5.1. Conclusions

The model that Krijger (2013) implemented has been extended to include the effects of thermal inertia in the wall of the heating section. Several instability characteristics have been computed from the model for a reference case and parametric studies have been performed on the wall cross-section, wall thermal conductivity and the simultaneous scaling of the channel flow area and hydraulic diameter. From the results the following conclusions are drawn.

The introduction of core wall thermal inertia to the system initially has a stabilizing effect, but as the wall cross-section is increased the stability declines in the high pseudo phase change-high sub-cooling region. Eventually, at a wall cross-section of about ten times the channel flow area, this recession stagnates. Three instability regions are identified, one being almost completely overlapped by a Ledinegg instability region, the other two distinguished by a conflict of instability regimens, as indicated by a study on the resonance frequencies. The Ledinegg instability region that overlaps the first region extends into one of the latter two as well. The region that is overlapped by the Ledinegg instability region shows resemblance to the stability boundary found by T'Joen & Rohde (2012), albeit displaying no resonance frequencies, and its boundary shows the trend that Schenderling (2013) discovered as well.

When the wall is scaled up, two new instability regions emerge in low power areas, one bordering the single-phase flow region and the other occurring at a slightly higher power. The former contains low (probably gravitation driven) resonance frequencies whereas the latter is more friction driven. The newly found regions meet at zero sub-cooling and zero pseudo phase change. At least one of the newly found unstable regions also appears if the channel hydraulic diameter and flow area are scaled down, namely the region corresponding to the low-frequency region. The newly found regions contain no Ledinegg instabilities.

The possibility that the stability decline occurs due to the increased axial heat conduction from the larger wall cross-section is ruled out, as the axial thermal conductivity was found to have very little influence on the neutral stability boundary.

It is also concluded that the steady state, and thereby the occurrence of the Ledinegg instability regions, is almost independent of the wall cross-section, as, in steady state, it depends only on the axial heat conduction which itself is not very significant to the system.

The specific enthalpy-dependent modelling of the coolant thermal conductivity was investigated as well. This was found to have a more significant effect, as the stability boundary recedes less in the case of a constant coolant thermal conductivity. It suggests that the perturbations in coolant thermal conductivity at least partly account for the recession of the stability boundary for larger wall cross-sections.

5.2. Discussion and Recommendations

The fact that the enthalpy-dependent modelling of the thermal conductivity of the coolant fluid had a significant effect on the behaviour of the neutral stability boundary leaves open several questions regarding the modelling of thermodynamic properties of the fluid in general. For instance, the dynamic viscosity is assumed constant in this thesis, but varies with specific enthalpy as well. It may be subjected to a simple parametric study to find out the significance of its variability.

In this thesis perturbations in the coolant thermal conductivity were taken into account both in the steady state calculations and in the transient calculations. Several other dependencies were only taken into account in the steady state calculations, such as the specific heat dependency of the Prandtl number. For the sake of completeness one may want to set up a more accurate model, but this will be at the cost of the system's simplicity and it may be very time consuming. Again, a parametric study may be performed to determine the significance of such modifications.

In this thesis, the core channel had been modelled as consisting of either one or two nodes, depending on the operational conditions. This had been done for the core wall as well. In the model that assumes two core nodes, the temperature gradient in the wall was calculated between the centres of the wall nodes. The top wall node was modelled to exchange heat with the core channel at the same height. This modelling is not accurate, as the fluid properties in the top channel node were specified at the top of the node, rather than in the centre. The implementation of additional dependencies on the perturbed node lengths may be necessary for the sake of accuracy.

The code used in this thesis is limited in the sense that is does not allow for the axial heat conduction among the wall nodes to influence the system significantly. The set of iterative calculations leaves room for improvement.

This thesis extended Krijger's (2013) thesis by the implementation of thermal inertia effects from the core wall. Another implementation suggested by Krijger is to implement neutronic-thermal-hydraulic coupling as well.

In this thesis, whether the system is stable at given operational conditions is dependent on the solution to an eigenvalue problem. If all eigenvalues have a real part that is negative, then the system is considered stable (not including Ledinegg instabilites). Instability maps generated by the code do not show which eigenvalues are positive at unstable conditions. It is, however, possible to make the code display which eigenvalues are responsible for destabilizing the system. The information yielded by this implementation may be useful for a more thorough understanding of the system mechanics.

BIBLIOGRAPHY

--Bouré, J., Bergles, A., Tong, L. (1973), Review of two phase flow instability. *Nuclear Engineering and Design 25*

--Generation IV International Forum (2013), *GEN-4 : Technology : Systems*, viewed 25 November 2013, <http://www.gen-4.org/Technology/systems/index.htm>

--Guido, G., Converti, J., Clausse, A. (1991), Density-wave oscillations in parallel channels – an analytical approach, *Nuclear Engineering and Design 125*

--Jain, P., Rizwan-Uddin (2008), Numerical analysis of supercritical flow instabilities, *Nuclear Engineering and Design 238-8*

--Kam, F. (2011), *Development of a one-dimensional model for the stability analysis of a natural circulation Super Critical Water Reactor,* M.Sc. thesis, TU Delft

--Koren, G. (2010), *Linear Stability Analysis of a Supercritical Water Loop driven by Natural Convection*, B.Sc. thesis, TU Delft

--Krijger, D. (2013), *A lnear stability analysis of a water loop driven by natural convection at supercritical conditions*, B.Sc. thesis, TU Delft

--Lomperski, S., Cho, D., Jain, R., Corradini, M. (2004), Stability of a natural circulation loop with a fluid heated through thermodynamic pseudo-critical point. *Proceedings of the 2004 International Congress on Advances in Nuclear Power Plants, ICAPP'04*

--Marcel, C. (2007), *Experimental and numerical stability investigations on natural circulation boiling water reactors*, Ph.D. dissertation, TU Delft

--NIST (2013), *Thermophysical Properties of Fluid Systems,* viewed 24 October 2013, <http://webbook.nist.gov/chemistry/fluid/>

--Ortega Gómez, T. (2009), *Stability Analysis of the High Performance Light Water Reactor*, Ph.D. dissertation, Institut für Kern- und Energietechnik

--Schenderling, T. (2013), *Numerical analysis of the influence of wall thermal inertia on the stability of natural circulation driven supercritical water reactors,* B.Sc. thesis, TU Delft

--Spoelstra, J. (2012), *Numerical stability analysis of natural circulation driven supercritical water reactors*, M.Sc. thesis, TU Delft

--T'Joen, C., Rohde, M. (2012), Experimental study of the coupled thermo-hydraulic-neutronic stability of a natural circulation HPLWR. *Nuclear Engineering and Design 242*

--Van Bragt, D. (1998), *Analytical modeling of boiling water reactor dynamics*, Ph.D. dissertation, Interfaculty Reactor Institute

--Van Den Akker, H., Mudde, R. (1996), *Fysische Transportverschijnselen*, 3rd edition, VSSD

NOMENCLATURE

Roman characters

A	[m^2]	Channel flow area
A_w	[m^2]	Wall cross-sectional area
D_H	[m]	Hydraulic diameter
H	[J kg^{-1}]	Specific enthalpy
K	[]	Pressure loss coefficient
L	[m]	Length
P_{in}	[m]	Perimeter
Q	[J s^{-1}]	Core heating
T	[^oC]	Temperature
V	[m^3]	Volume
W	[kg s^{-1}]	Mass flow rate
c_p	[J kg^{-1} K^{-1}]	Fluid specific heat
$c_{p,w}$	[J kg^{-1} K^{-1}]	Wall material specific heat
f		Darcy friction factor
g	[m s^{-2}]	Gravitational acceleration
h	[J kg^{-1}]	Specific enthalpy
p	[Pa]	Pressure
q	[J s^{-1}]	Heat loss
t	[s]	Time

Greek characters

θ	[K]	Temperature (perturbation)
λ		Eigenvalue
λ_f	[W m^{-1} K^{-1}]	Fluid thermal conductivity
λ_w	[W m^{-1} K^{-1}]	Wall thermal conductivity
μ	[Pa s]	Dynamic viscosity
ρ	[kg m^{-3}]	Fluid density
ρ_w	[kg m^{-3}]	Wall material density
υ	[m^3 kg^{-1}]	Fluid specific volume

Other

$\bar{X}$		Steady state variable
$\underline{X}$		Dimensionless variable
$\breve{x}$		Perturbation
$\widehat{Nu}$	[$W^{0.66}$ $m^{-0.66}$ $K^{-0.66}$]	Adjusted Nusselt number

Dimensionless numbers

N_{sub}	Sub-cooling number
$N_{\Delta h}$	Pseudo phase change number
N_{Fr}	Froude number
Re	Reynolds number

Pr	Prandtl number
Nu	Nusselt number

Subscripts

0	Value at the bottom core node
1	Value at the top core node
R	Value in the riser node
B	Value in the buffer vessel
D	Value in the downcomer
pc	Value at the pseudo-critical point
w	Value in the wall (low heating model)
w,0	Value in bottom wall node (high heating model)
w,1	Value in top wall node (high heating model)

Common abbreviations

BWR	Boiling Water Reactor
DR	Decay Ratio
HPLWR	High Performance Light Water Reactor
LWR	Light Water Reactor
NSB	Neutral Stability Boundary
PWR	Pressurized Water Reactor
SCWR	Supercritical Water-cooled Reactor

APPENDIX A. BALANCE EQUATIONS (KRIJGER, 2013)

Throughout this thesis, several references are made to the balance equations of Krijger's (2013) interpretation of the supercritical water loop model. In this Appendix these transport balance equations are summarized.

The underline in the left column is used to refer to the equations. An M is used to refer to a mass balance, an E for an energy (heat) balance and an I for a momentum balance. The momentum balance I is the momentum balance for the entire loop, while mass and heat balances are constituted for single nodes. That is why all mass and heat balance characters M and E are followed by a character specifying the node to which the balance equation applies. For example, the mass balance of the riser node is denoted MR, M for mass, R for riser.

In dimensionless equations the underline is used to refer to the dimensionless version of the variable, of which the explanation is given in Table 2.1. A variable X is denoted $\breve{x}$ if a perturbation is meant. Steady state variables X are denoted $\overline{X}$.

A.1. Low heating model – Transport balances

M0: $$AL\frac{d}{dt}\rho_0 = W_0 - W_{out} \quad \textbf{(A.1)}$$

MR: $$AL_R\frac{d}{dt}\rho_R = W_{out} - W_R \quad \textbf{(A.2)}$$

MB: $$\rho_{IN}\frac{d}{dt}V_B = W_R - W_0 \quad \textbf{(A.3)}$$

E0: $$AL\frac{d}{dt}\rho_0 H_0 = W_0 H_{IN} - W_{out}H_{out} + Q \quad \textbf{(A.4)}$$

ER: $$AL_R\frac{d}{dt}\rho_R H_R = W_{out}H_{out} - W_R H_R \quad \textbf{(A.5)}$$

I: $$AL\frac{d}{dt}W_0 + AL_R\frac{d}{dt}W_R + \frac{d}{dt}V_B W_0 + AL_D\frac{d}{dt}W_0 = -\frac{1}{2}\left(\frac{f_0 L}{D_H} + K_0\right)\frac{W_0^2}{\rho_0} \ldots$$

$$\ldots -\frac{1}{2}\left(\frac{f_R L_R}{D_H} + K_R\right)\frac{W_R^2}{\rho_R} - \frac{1}{2}\left(\frac{f_D L_D}{D_H} + K_D\right)\frac{W_0^2}{\rho_{IN}} - A^2 g\rho_0 L - A^2 g\rho_R L_R - A^2 g\rho_{IN} L_D \quad \textbf{(A.6)}$$

A.2. High heating model – Transport balances

M0: $$A\rho_0\frac{d}{dt}L_0 = W_0 - W_{pc} \quad \textbf{(A.7)}$$

M1: $$A\frac{d}{dt}\rho_1 L_1 = W_{pc} - W_1 \quad \textbf{(A.8)}$$

MR: $$AL_R\frac{d}{dt}\rho_R = W_1 - W_R \quad \textbf{(A.9)}$$

MB: $$\rho_{IN}\frac{d}{dt}V_B = W_R - W_0 \quad \textbf{(A.10)}$$

E0: $$A\rho_0 H_0\frac{d}{dt}L_0 = W_0 H_{in} - W_{pc}h_{pc} + Q\frac{L_0}{L} \quad \textbf{(A.11)}$$

E1: $$A\frac{d}{dt}\rho_1 L_1 H_1 = W_{pc}h_{pc} - W_1 H_1 + Q\frac{L_1}{L} \quad \textbf{(A.12)}$$

ER: $$AL_R\frac{d}{dt}\rho_R H_R = W_1 H_1 - W_R H_R \quad \textbf{(A.13)}$$

I: $$A\frac{d}{dt}W_0 L_0 + A\frac{d}{dt}W_1 L_1 + AL_R\frac{d}{dt}W_R + \frac{d}{dt}V_B W_0 + AL_D\frac{d}{dt}W_0 = \cdots$$
$$\cdots - \frac{1}{2}\left(\frac{f_0 L_0}{D_H} + K_0\right)\frac{W_0^2}{\rho_0} - \frac{1}{2}\left(\frac{f_1 L_1}{D_H} + K_1\right)\frac{W_1^2}{\rho_1} - \frac{1}{2}\left(\frac{f_R L_R}{D_H} + K_R\right)\frac{W_R^2}{\rho_R}\cdots$$
$$\cdots - \frac{1}{2}\left(\frac{f_D L_D}{D_H} + K_D\right)\frac{W_0^2}{\rho_{IN}} - A^2 g\rho_0 L_0 - A^2 g\rho_1 L_1 - A^2 g\rho_R L_R - A^2 g\rho_{IN} L_D \quad \textbf{(A.14)}$$

A.3. Low heating model – Dimensionless balances

M0: $$\frac{d}{d\underline{t}}\underline{\rho}_0 = \underline{W}_0 - \underline{L}_R\frac{d}{d\underline{t}}\underline{\rho}_R - \underline{W}_R \quad \textbf{(A.15)}$$

E0: $$\frac{d}{d\underline{t}}\underline{\rho}_0\underline{H}_0 = \underline{W}_0\underline{H}_{in} - \underline{H}_{out}\left(\underline{L}_R\frac{d}{d\underline{t}}\underline{\rho}_R + \underline{W}_R\right) + 1 \quad \textbf{(A.16)}$$

ER: $$\underline{L}_R\frac{d}{dt}\underline{\rho}_R\underline{H}_R = \underline{H}_{out}\left(\underline{L}_R\frac{d}{d\underline{t}}\underline{\rho}_R + \underline{W}_R\right) - \underline{W}_R\underline{H}_R \quad \textbf{(A.17)}$$

I: $$\frac{d}{d\underline{t}}\underline{W}_0 + \underline{L}_R\frac{d}{d\underline{t}}\underline{W}_R + \underline{V}_B\frac{d}{d\underline{t}}\underline{W}_0 + \underline{L}_D\frac{d}{d\underline{t}}\underline{W}_0 = -\underline{W}_0\frac{\underline{W}_R - \underline{W}_0}{\underline{\rho}_{IN}} - \frac{1}{2}\left(\frac{f_0}{\underline{D}_H} + K_0\right)\frac{\underline{W}_0{}^2}{\underline{\rho}_0}\cdots$$
$$\cdots - \frac{1}{2}\left(\frac{f_R\underline{L}_R}{\underline{D}_H} + K_R\right)\frac{\underline{W}_R{}^2}{\underline{\rho}_R} - \frac{1}{2}\left(\frac{f_D\underline{L}_D}{\underline{D}_H} + K_D\right)\frac{\underline{W}_0{}^2}{\underline{\rho}_{in}} - \frac{\underline{\rho}_0\underline{L}_0}{N_{Fr}} - \frac{\underline{\rho}_R\underline{L}_R}{N_{Fr}} + \frac{\underline{\rho}_{in}\underline{L}_D}{N_{Fr}} \quad \textbf{(A.18)}$$

A.4. High heating model – Dimensionless balances

M0: $$\underline{\rho}_0\left(\frac{\underline{H}_0}{\underline{h}_{pc}} - 1\right)\frac{d}{d\underline{t}}\underline{L}_1 = \left(1 - \frac{\underline{H}_{in}}{\underline{h}_{pc}}\right)\underline{W}_0 - \frac{1}{\underline{h}_{pc}}\left(1 - \underline{L}_1\right) \quad \textbf{(A.19)}$$

M1: $$\left(\underline{\rho}_1 - \frac{\underline{H}_0}{\underline{h}_{pc}}\underline{\rho}_0\right)\frac{d}{d\underline{t}}\underline{L}_1 + \underline{L}_1\frac{d}{d\underline{t}}\underline{\rho}_1 = \frac{\underline{H}_{in}}{\underline{h}_{pc}}\underline{W}_0 + \frac{1}{\underline{h}_{pc}}\left(1 - \underline{L}_1\right) - \underline{W}_1 \quad \textbf{(A.20)}$$

MR: $$\underline{L}_R\frac{d}{d\underline{t}}\underline{\rho}_R = \underline{W}_1 - \underline{W}_R \quad \textbf{(A.21)}$$

E1: $$\underline{L}_1\frac{d}{d\underline{t}}\underline{\rho_1 H_1} + \left(\underline{\rho_1 H_1} - \underline{\rho_0 H_0}\right)\frac{d}{d\underline{t}}\underline{L}_1 = \underline{W_0 H_{in}} - \underline{W_1 H_1} + 1 \quad \textbf{(A.22)}$$

ER: $$\underline{L_R}\frac{d}{d\underline{t}}\underline{\rho_R H_R} = \underline{W_1 H_1} - \underline{W_R H_R} \quad \textbf{(A.23)}$$

I: $$-\underline{W_0}\frac{d}{d\underline{t}}\underline{L_1}+\left(1-\underline{L_1}\right)\frac{d}{d\underline{t}}\underline{W_0}+\frac{d}{d\underline{t}}\underline{W_1}\underline{L_1}+\underline{L_R}\frac{d}{d\underline{t}}\underline{W_R}+\underline{V_B}\frac{d}{d\underline{t}}\underline{W_0}+\underline{L_D}\frac{d}{d\underline{t}}\underline{W_0}\ \dots$$
$$\dots=-\underline{W_0}\frac{\underline{W_R}-\underline{W_0}}{\underline{\rho_{IN}}}-\frac{1}{2}\left(\frac{f_0\underline{L_0}}{\underline{D_H}}+K_0\right)\frac{\underline{W_0}^2}{\underline{\rho_0}}-\frac{1}{2}\left(\frac{f_1\underline{L_1}}{\underline{D_H}}+K_1\right)\frac{\underline{W_1}^2}{\underline{\rho_1}}-\frac{1}{2}\left(\frac{f_R\underline{L_R}}{\underline{D_H}}+K_R\right)\frac{\underline{W_R}^2}{\underline{\rho_R}}$$
$$\dots\frac{1}{2}\left(\frac{f_D\underline{L_D}}{\underline{D_H}}+K_D\right)\frac{\underline{W_0}^2}{\underline{\rho_{in}}}-\frac{\underline{\rho_0}\underline{L_0}}{N_{Fr}}-\frac{\underline{\rho_1}\underline{L_1}}{N_{Fr}}-\frac{\underline{\rho_R}\underline{L_R}}{N_{Fr}}+\frac{\underline{\rho_{in}}\underline{L_D}}{N_{Fr}} \quad \textbf{(A.24)}$$

A.5. Low heating model – Linearized balances

M0: $$C_1N_{\Delta h}h_{pc}v_{pc}\left(\frac{1}{2}\frac{d}{d\underline{t}}\breve{\underline{h}}_{out}+\underline{L_R}\frac{d}{d\underline{t}}\breve{\underline{h}}_R\right)=\breve{\underline{w}}_0-\breve{\underline{w}}_R \quad \textbf{(A.25)}$$

E0: $$\left(\frac{1}{2}\overline{\underline{\rho_0}}+\frac{1}{2}C_1N_{\Delta h}h_{pc}v_{pc}\overline{\underline{H_0}}\right)\frac{d}{d\underline{t}}\breve{\underline{h}}_{out}+C_1N_{\Delta h}h_{pc}v_{pc}\overline{\underline{H_{out}}}\underline{L_R}\frac{d}{d\underline{t}}\breve{\underline{h}}_R=\cdots$$
$$\dots-\overline{\breve{w}_R}\overline{\underline{H_{out}}}+\overline{\breve{w}_0}\overline{\underline{H_{in}}}-\breve{\underline{h}}_{out} \quad \textbf{(A.26)}$$

ER: $$\left(\underline{L_R}\overline{\underline{\rho_R}}-\underline{L_R}C_1N_{\Delta h}h_{pc}v_{pc}\left(\overline{\underline{H_R}}-\overline{\underline{H_{out}}}\right)\right)\frac{d}{d\underline{t}}\breve{\underline{h}}_R=\breve{\underline{h}}_{out}+\overline{\underline{H_{out}}}\breve{\underline{w}}_R-\breve{\underline{h}}_R-\breve{\underline{w}}_R\overline{\underline{H_R}} \quad \textbf{(A.27)}$$

I: $$\left(1+\underline{L_D}+\underline{V_B}\right)\frac{d}{d\underline{t}}\breve{\underline{w}}_0+\underline{L_R}\frac{d}{d\underline{t}}\breve{\underline{w}}_R=-\left(\left(\frac{f_R\underline{L_R}}{\underline{D_H}}+K_R\right)\overline{\underline{v}}_R+\underline{v_{in}}\right)\breve{\underline{w}}_R+\cdots$$
$$\dots\frac{1}{2}\left(\frac{1}{2}\left(\frac{f_0}{\underline{D_H}}+K_0\right)\frac{1}{\overline{\underline{\rho_0}}^2}-\frac{1}{N_{Fr}}\right)C_1N_{\Delta h}h_{pc}v_{pc}\breve{\underline{h}}_{out}+\left(\frac{1}{2}\left(\frac{f_R\underline{L_R}}{\underline{D_H}}+K_R\right)\frac{1}{\overline{\underline{\rho_R}}^2}-\frac{\underline{L_R}}{N_{Fr}}\right)C_1N_{\Delta h}h_{pc}v_{pc}\breve{\underline{h}}_R+\dots$$
$$\dots\left(\underline{v_{in}}\left(\frac{f_0}{\underline{D_H}}+K_0\right)\overline{\underline{v}}_0-\left(\frac{f_D\underline{L_D}}{\underline{D_H}}+K_D\right)\underline{v_{in}}\right)\breve{\underline{w}}_0 \quad \textbf{(A.28)}$$

A.6. High heating model – Linearized balances

M0: $$\underline{\rho_0}\left(\frac{\underline{H_0}}{\underline{h_{pc}}}-1\right)\frac{d}{d\underline{t}}\breve{\underline{l}}_1=\left(1-\frac{\underline{H_{in}}}{\underline{h_{pc}}}\right)\breve{\underline{w}}_0+\frac{1}{\underline{h_{pc}}}\breve{\underline{l}}_1 \quad \textbf{(A.29)}$$

M1: $$\left(\frac{1}{\overline{\underline{v_1}}}-\frac{\underline{H_0}}{\underline{h_{pc}}}\underline{\rho_0}\right)\frac{d}{d\underline{t}}\breve{\underline{l}}_1-\frac{\overline{\underline{L_1}}C_1N_{\Delta h}h_{pc}}{v_{pc}\overline{\underline{v_1}}^2}\frac{d}{d\underline{t}}\breve{\underline{h}}_1=\frac{\underline{H_{in}}}{\underline{h_{pc}}}\breve{\underline{w}}_0-\frac{1}{\underline{h_{pc}}}\breve{\underline{l}}_1-\breve{\underline{w}}_1 \quad \textbf{(A.30)}$$

MR: $$-\frac{\overline{\underline{L_R}}C_1N_{\Delta h}h_{pc}}{v_{pc}\overline{\underline{v_R}}^2}\frac{d}{d\underline{t}}\breve{\underline{h}}_R=\breve{\underline{w}}_1-\breve{\underline{w}}_R \quad \textbf{(A.31)}$$

E1: $$\frac{\overline{\underline{L_1}}}{\overline{\underline{v_1}}}\left(1-\frac{N_{\Delta h}C_1h_{pc}\overline{\underline{H_1}}}{v_{pc}\overline{\underline{v_1}}}\right)\frac{d}{d\underline{t}}\widetilde{\underline{h_1}}+\left(\frac{\overline{\underline{H_1}}}{\overline{\underline{v_1}}}-\underline{H_0\rho_0}\right)\frac{d}{d\underline{t}}\breve{\underline{l}}_1=\underline{H_{in}\breve{w}_0}-\overline{\underline{H_1}}\overline{\breve{w}_1}-\widetilde{\underline{h_1}} \quad \textbf{(A.32)}$$

ER: $$\frac{\overline{\underline{L_R}}}{\overline{\underline{v_R}}}\left(1-\frac{N_{\Delta h}C_1h_{pc}\overline{\underline{H_R}}}{v_{pc}\overline{\underline{v_R}}}\right)\frac{d}{d\underline{t}}\widetilde{\underline{h_R}}=\widetilde{\underline{h_1}}+\overline{\underline{H_1}}\overline{\breve{w}_1}-\widetilde{\underline{h_R}}-\overline{\underline{H_R}}\overline{\breve{w}_R} \quad \textbf{(A.33)}$$

$$\underline{\text{I:}} \qquad \left(\mathbf{1}-\overline{\underline{L_1}}+\underline{L_D}+\underline{V_B}\right)\frac{d}{d\underline{t}}\breve{\underline{w}}_0+\overline{\underline{L_1}}\,\frac{d}{d\underline{t}}\breve{\underline{w}}_1+\underline{L_R}\,\frac{d}{d\underline{t}}\breve{\underline{w}}_R=\cdots$$

$$\cdots\left(\frac{1}{2}\left(\frac{f_0\underline{v_0}}{\underline{D_H}}-\frac{f_1\overline{\underline{v}}_1}{\underline{D_H}}\right)+\frac{1}{N_{Fr}\underline{v_0}}-\frac{1}{N_{Fr}\overline{\underline{v}}_1}\right)\breve{\underline{l}}_1-\left(\left(\frac{f_0\overline{\underline{L}}_0}{\underline{D_H}}+\boldsymbol{K_0}\right)\underline{v_0}+\left(\frac{f_D\underline{L_D}}{\underline{D_H}}+\boldsymbol{K_D}\right)\underline{v_{in}}-\underline{v_{in}}\right)\breve{\underline{w}}_0\cdots$$

$$\cdots\left(\frac{f_1\overline{\underline{L_1}}}{\underline{D_H}}+\boldsymbol{K_1}\right)\overline{\underline{v_1}}\breve{\underline{w}}_1+\left(-\frac{1}{2}\left(\frac{f_1\overline{\underline{L_1}}}{\underline{D_H}}+\boldsymbol{K_1}\right)+\frac{\overline{\underline{L_1}}}{N_{Fr}\overline{\underline{v}}_1{}^2}\right)\frac{N_{\Delta h}C_1h_{pc}}{v_{pc}}\widetilde{\underline{h_1}}\cdots$$

$$\cdots-\left(\frac{f_R\underline{L_R}}{\underline{D_H}}+\boldsymbol{K_R}+\frac{\underline{v_{in}}}{\overline{\underline{v_R}}}\right)\overline{\underline{v_R}}\breve{\underline{w}}_R+\left(-\frac{1}{2}\left(\frac{f_R\underline{L_R}}{\underline{D_H}}+\boldsymbol{K_R}\right)+\frac{\underline{L_R}}{N_{Fr}\overline{\underline{v}}_R{}^2}\right)\frac{N_{\Delta h}C_1h_{pc}}{v_{pc}}\widetilde{\underline{h_R}} \qquad \textbf{(A.34)}$$

APPENDIX B. COEFFICIENT MATRICES

B.1. Low heating model

Coefficient matrix A

$$\begin{Bmatrix} \frac{1}{2}C_1 N_{\Delta h} h_{pc} \upsilon_{pc} & C_1 N_{\Delta h} h_{pc} \upsilon_{pc} \underline{L_R} & 0 & 0 & 0 \\ \frac{1}{2}\left(C_1 N_{\Delta h} h_{pc} \upsilon_{pc} \overline{\underline{H_0}} + \underline{\rho_0}\right) & C_1 N_{\Delta h} h_{pc} \upsilon_{pc} \overline{\underline{H_{out}}}\, \underline{L_R} & 0 & 0 & 0 \\ 0 & \underline{L_R}\,\overline{\underline{\rho_R}} + \underline{L_R} C_1 N_{\Delta h} h_{pc} \upsilon_{pc} \left(\overline{\underline{H_R}} - \overline{\underline{H_{out}}}\right) & 0 & 0 & 0 \\ 0 & 0 & 1 + \underline{L_D} + \overline{\underline{V_B}} & \underline{L_R} & 0 \\ 0 & 0 & 0 & 0 & \underline{\rho_w} \underline{c_{p,w}} \underline{A_w} \end{Bmatrix}$$

Coefficient matrix B

Columns 1,2

$$\begin{Bmatrix} 0 & 0 \\ -\left(\underline{Nu_0}\,\frac{\underline{P_{in}}}{\underline{D_H}}\left(\left(\underline{\alpha_0}\left(\underline{H_0} - \underline{h_{pc}}\right) + \frac{1}{2\underline{c_{p,pc}}}\right)\overline{\underline{\lambda_{f0}}}^{0.34} - 0{,}17\,\underline{\lambda_{f0}}^{-0.66}\left(\overline{\underline{T_w}} - \overline{\underline{T_0}}\right)\underline{\beta_0}\right) + 1\right) & 0 \\ 1 & -1 \\ \frac{1}{2}\left(\frac{1}{2}\left(\frac{\underline{f_0}}{\underline{D_H}} + K_0\right)\frac{1}{\underline{\underline{\rho_0^2}}} - \frac{1}{N_{Fr}}\right) C_1 N_{\Delta h} h_{pc} \upsilon_{pc} & \frac{1}{2}\left(\frac{1}{2}\left(\frac{f_R \underline{L_R}}{\underline{D_H}} + K_R\right)\frac{1}{\underline{\underline{\rho_R^2}}} - \frac{\underline{L_R}}{N_{Fr}}\right) C_1 N_{\Delta h} h_{pc} \upsilon_{pc} \\ \frac{1}{2}\,\underline{Nu_0}\,\frac{\underline{P_{in}}}{\underline{D_H}}\left(\overline{\underline{\lambda_{f0}}}^{0.34}\left(2\underline{\alpha_0}\left(\underline{H_0} - \underline{h_{pc}}\right) + \frac{1}{\underline{c_{p,pc}}}\right) - 0{,}34\,\overline{\underline{\lambda_{f0}}}^{-0.66}\left(\overline{\underline{T_w}} - \overline{\underline{T_0}}\right)\underline{\beta_0}\right) & 0 \end{Bmatrix}$$

Columns 3,4,5

$$\begin{Bmatrix} 1 & -1 & 0 \\ \overline{\underline{H_{in}}} & -\overline{\underline{H_{out}}} & \underline{Nu_0}\,\overline{\underline{\lambda_{f0}}}^{0.34}\,\frac{\underline{P_{in}}}{\underline{D_H}} \\ 0 & \overline{\underline{H_{out}}} - \overline{\underline{H_R}} & 0 \\ \left(\underline{\upsilon_{IN}} - \left(\frac{\underline{f_0}}{\underline{D_H}} + K_0\right)\overline{\underline{\upsilon_0}} - \left(\frac{\underline{f_D}\,\underline{L_D}}{\underline{D_H}} + K_D\right)\underline{\upsilon_{IN}}\right) & -\left(\left(\frac{\underline{f_R}\,\underline{L_R}}{\underline{D_H}} + K_R\right)\overline{\underline{\upsilon_R}} + \underline{\upsilon_{IN}}\right) & 0 \\ 0 & 0 & -\underline{Nu_0}\,\overline{\underline{\lambda_{f0}}}^{0.34}\,\frac{\underline{P_{in}}}{\underline{D_H}} \end{Bmatrix}$$

B.2. High heating model

Coefficient matrix A

$$\begin{Bmatrix}
\underline{\rho_0}\left(\frac{\underline{\underline{H_0}}}{\underline{h_{pc}}}-1\right) & 0 & 0 & 0 & 0 & 0 & 0 & 0 \\
\frac{1}{\underline{\underline{\upsilon_1}}}-\frac{\underline{\underline{H_0}}}{\underline{h_{pc}}}\underline{\rho_0} & -\frac{\overline{\underline{L_1}}\underline{\underline{N_{\Delta h}}}\underline{C_1}\underline{h_{pc}}}{\underline{\upsilon_{pc}}\,\overline{\underline{\upsilon_1^2}}} & 0 & 0 & 0 & 0 & 0 & 0 \\
0 & 0 & -\frac{\underline{L_R}\underline{N_{\Delta h}}\underline{C_1}\underline{h_{pc}}}{\underline{\upsilon_{pc}}\,\overline{\underline{\upsilon_R^2}}} & 0 & 0 & 0 & 0 & 0 \\
\left(\frac{\overline{\underline{H_1}}}{\underline{\underline{\upsilon_1}}}-\underline{H_0}\,\underline{\rho_0}\right) & \frac{\overline{\underline{L_1}}}{\underline{\underline{\upsilon_1}}}\left(1-\frac{\underline{N_{\Delta h}}\underline{C_1}\underline{h_{pc}}\,\overline{\underline{H_1}}}{\underline{\upsilon_{pc}}\,\overline{\underline{\upsilon_1}}}\right) & 0 & 0 & 0 & 0 & 0 & 0 \\
0 & 0 & \frac{\underline{L_R}}{\underline{\underline{\upsilon_R}}}\left(1-\frac{\underline{N_{dh}}\underline{C_1}\underline{h_{pc}}\,\overline{\underline{H_R}}}{\underline{\upsilon_{pc}}\,\overline{\underline{\upsilon_R}}}\right) & 0 & 0 & 0 & 0 & 0 \\
0 & 0 & 0 & 1-\overline{\underline{L_1}}+\underline{L_D}+\overline{\underline{V_B}} & \overline{\underline{L_1}} & \underline{L_R} & 0 & 0 \\
-\underline{\rho_w}\underline{c_{p,w}}\underline{A_w}\,\overline{\underline{T_{w,0}}} & 0 & 0 & 0 & 0 & 0 & \underline{\rho_w}\underline{c_{p,w}}\underline{A_w}\,\overline{\underline{L_0}} & 0 \\
\underline{\rho_w}\underline{c_{p,w}}\underline{A_w}\,\overline{\underline{T_{w,1}}} & 0 & 0 & 0 & 0 & 0 & 0 & \underline{\rho_w}\underline{c_{p,w}}\underline{A_w}\,\overline{\underline{L_1}}
\end{Bmatrix}$$

Coefficient matrix B

Columns 1,2

$$\begin{Bmatrix}
\frac{1}{\underline{h_{pc}}} & 0 \\
-\frac{1}{\underline{h_{pc}}} & 0 \\
0 & 0 \\
\frac{\underline{P_{in}}}{\underline{D_H}}\left(\underline{Nu_1}\,\overline{\underline{\lambda_{f1}^{0.34}}}\left(\overline{\underline{T_{w,1}}}-\overline{\underline{T_1}}\right)-\underline{Nu_0}\,\overline{\underline{\lambda_{f0}^{0.34}}}\left(\overline{\underline{T_{w,0}}}-\underline{T_0}\right)\right) & -\left(\underline{Nu_1}\,\frac{\underline{P_{in}}\,\overline{\underline{L_1}}}{\underline{\underline{D_H}}}\left(\left(2\underline{\alpha_1}\left(\underline{H_1}-\underline{h_{pc}}\right)+\frac{1}{\underline{c_{p,pc}}}\right)\overline{\underline{\lambda_{f1}^{0.34}}}+0,34\left(\overline{\underline{T_{w,1}}}-\overline{\underline{T_1}}\right)\overline{\underline{\lambda_{f1}^{-0,66}}}\,\underline{\beta_1}\,\underline{\lambda_z}e^{-\underline{\beta_1}\overline{\underline{H_1}}}\right)+1\right) \\
0 & 1 \\
\frac{1}{2}\left(\frac{\underline{f_0}\,\underline{\upsilon_0}}{\underline{D_H}}-\frac{\underline{f_1}\,\overline{\underline{\upsilon_1}}}{\underline{D_H}}\right)+\frac{1}{\underline{\upsilon_0}\underline{N_{Fr}}}-\frac{1}{\underline{N_{Fr}}\,\overline{\underline{\upsilon_1}}} & \left(-\frac{1}{2}\left(\frac{\underline{f_1}\,\overline{\underline{L_1}}}{\underline{D_H}}+K_1\right)+\frac{\overline{\underline{L_1}}}{\underline{\underline{\upsilon_1^2}}\underline{N_{Fr}}}\right)\frac{\underline{N_{\Delta h}}\underline{C_1}\underline{h_{pc}}}{\underline{\upsilon_{pc}}} \\
\left(\underline{Nu_0}\,\overline{\underline{\lambda_{f0}^{0.34}}}\,\frac{\underline{P_{in}}}{\underline{D_H}}\left(\overline{\underline{T_{w,0}}}-\underline{T_0}\right)-1\right) & 0 \\
\left(1-\underline{Nu_1}\,\overline{\underline{\lambda_{f1}^{0.34}}}\,\frac{\underline{P_{in}}}{\underline{D_H}}\left(\overline{\underline{T_{w,1}}}-\overline{\underline{T_1}}\right)\right) & \underline{Nu_1}\,\frac{\underline{P_{in}}\,\overline{\underline{L_1}}}{\underline{\underline{D_H}}}\left(\left(2\underline{\alpha_1}\left(\overline{\underline{H_1}}-\underline{h_{pc}}\right)+\frac{1}{\underline{c_{p,pc}}}\right)\overline{\underline{\lambda_{f1}^{0.34}}}+0,34\left(\overline{\underline{T_{w,1}}}-\overline{\underline{T_1}}\right)\overline{\underline{\lambda_{f1}^{-0,66}}}\,\underline{\beta_1}\,\underline{\lambda_z}e^{-\underline{\beta_1}\overline{\underline{H_1}}}\right)
\end{Bmatrix}$$

Columns 3,4,5

$$\begin{Bmatrix} 0 & 1-\frac{\underline{\underline{H_{IN}}}}{\underline{h_{pc}}} & 0 \\ 0 & \frac{\underline{\underline{H_{IN}}}}{\underline{h_{pc}}} & -1 \\ 0 & 0 & 1 \\ 0 & \underline{H_{IN}} & -\overline{\underline{H_1}} \\ -1 & 0 & \overline{\underline{H_1}} \\ \left(-\frac{1}{2}\left(\frac{\underline{f_R}\,\underline{\underline{L_R}}}{\underline{D_H}}+K_R\right)+\frac{\underline{\underline{L_R}}}{\underline{\underline{\upsilon_R^2}}\,N_{Fr}}\right)\frac{N_{\Delta h}C_1 h_{pc}}{\upsilon_{pc}} & -\left(\left(\frac{\underline{f_0}\,\overline{\underline{L_0}}}{\underline{D_H}}+K_0\right)\underline{\upsilon_0}+\left(\frac{\underline{f_D}\,\underline{L_D}}{\underline{D_H}}+K_D\right)\underline{\upsilon_{IN}}-\underline{\upsilon_{IN}}\right) & -\left(\frac{\underline{f_1}\,\overline{\underline{L_1}}}{\underline{D_H}}+K_1\right)\overline{\underline{\upsilon_1}} \\ 0 & 0 & 0 \\ 0 & 0 & 0 \end{Bmatrix}$$

Columns 6,7,8

$$\begin{Bmatrix} 0 & 0 & 0 \\ 0 & 0 & 0 \\ -1 & 0 & 0 \\ 0 & \underline{Nu_0}\,\overline{\underline{\lambda_{f0}^{0.34}}}\,\frac{\underline{\underline{P_{in}}}\,\overline{\underline{L_0}}}{\underline{D_H}} & \underline{Nu_1}\,\overline{\underline{\lambda_{f1}^{0.34}}}\,\frac{\underline{\underline{P_{in}}}\,\overline{\underline{L_1}}}{\underline{D_H}} \\ -\overline{\underline{H_R}} & 0 & 0 \\ -\left(\frac{\underline{f_R}\,\underline{\underline{L_R}}}{\underline{D_H}}+K_R+\frac{\upsilon_{IN}}{\underline{\underline{\upsilon_R}}}\right)\overline{\underline{\upsilon_R}} & 0 & 0 \\ 0 & -\left(\underline{Nu_0}\,\overline{\underline{\lambda_{f0}^{0.34}}}\,\frac{\underline{\underline{P_{in}}}\,\overline{\underline{L_0}}}{\underline{D_H}}+2\underline{\lambda_w}\,\underline{A_w}\right) & 2\underline{\lambda_w}\,\underline{A_w} \\ 0 & 2\underline{\lambda_w}\,\underline{A_w} & -\left(\underline{Nu_1}\,\overline{\underline{\lambda_{f1}^{0.34}}}\,\frac{\underline{\underline{P_{in}}}\,\overline{\underline{L_1}}}{\underline{D_H}}+2\underline{\lambda_w}\,\underline{A_w}\right) \end{Bmatrix}$$

APPENDIX C. REFERENCE CASE PARAMETERS

In this thesis several results are compared to those of a reference case, initially set up by Krijger (2013) and further extended in this thesis. This reference case is determined by the set of design parameters and material and thermodynamic properties that, for further investigation, are shown in this appendix. Gravitational acceleration is taken to be 9.81 $m.s^{-2}$.

Table C.1. Design parameters for the reference case

Parameter	**Value**
Volume buffer vessel	10 x_{10}^{-3} m^3
Riser length	4.2 m
Core length	4.2 m
Channel hydraulic diameter	5.6 x_{10}^{-3} m
Channel flow area	35.5 x_{10}^{-6} m^2
Wall cross-sectional area	35.5 x_{10}^{-6} m^2
Inlet pressure loss coefficient	1
Downcomer pressure loss coefficient	1
Riser pressure loss coefficient	20

Table C.2. Material and thermodynamic properties for the reference case

Property	**Value**
Water specific enthalpy, pseudo-critical point	2.1529 x_{10}^{6} J kg^{-1}
Water specific volume, pseudo-critical point	3.1564 x_{10}^{-3} m^3 kg^{-1}
Water specific heat capacity, pseudo-critical point	76444 W kg^{-1} K^{-1}
Dynamic viscosity of water	4.2797 x_{10}^{-5} Pa s
Wall density	7850 kg m^{-3}
Wall specific heat capacity	490 W kg^{-1} K^{-1}
Wall thermal conductivity	43 W m^{-1} K^{-1}

APPENDIX D. MATLAB CODES

D.1. Computation of dynamic instability map for reference case

```
% Dynamic instability map of natural circulation driven supercritical water
loop (Krijger, 2013) enhanced for core wall thermal inertia effects - Joris
Lippens
%Comments: Every constant or variable x is made dimensionless and denoted
%xt.

clc
clear all
close all
tic

dwres=1e-12;        %Accuracy of steady-state calculations
itlim=1e4;          %Limit of iterations for steady-state calculations

%GEOMETRY LOOP
L=4.2;
area=35.5e-6;
Lr=4.2;
Lrt=Lr./L;
Ld=Lr+L;
Ldt=Ld./L;
Vb=0.010;
Vbt=Vb./(area.*L);
D=5.6e-3;
Dt=D./L;
P_in=4.*area./D;          %Wetted perimeter of channel
P_int=P_in./L;
Aw=35.5e-6;               %Wall cross-section area
Awt=Aw./area;


%Friction coefficients
K0=1;
K1=0;
Kr=20;
Kd=1;

%CONSTANTS
N=100;
g=9.81;
hpc=2.1529e6;
vpc=0.0031564;
mu=4.2797e-5;           %Dynamic viscosity
C=0.80e-8;              %Coefficient linear specific volume
C2=-4.7877e-4;          %Coefficient linear density

aa0=-1.1e-10;           %Coefficient quadratic temperature node 0
aa1=1e-10;              %Coefficient quadratic temperature node 1
cppc=76444;
rrw=7850;               %Wall density
rrwt=rrw.*vpc;
Cpw=490;                %Wall specific heat
Tpc=tmpr(hpc);
```

```
llw=43;                 %Wall thermal conductivity

bb0=-3.2711e-7;         %Equation of state, coolant thermal conductivity
modelling
llb0=1.0133;
llb1=0.070154;
llz=4.555298930195932;
bb1=1.369367779861587e-06;
llpc=thermc(hpc);

llb0t=llb0./llpc;
llb1t=llb1./llpc;
llzt=llz./llpc;

ie=0;

SMAX=1;                 %Range of Nsub
PMAX=2;                 %Range of Ndh
Nsub=linspace(0.001,SMAX,N);
Ndh=linspace(0.001,PMAX,N);
Hin=hpc.*(1-Nsub);       %Inlet enthalpy
vin=specvol(Hin);        %Specifiv volume inlet
vint=vin./vpc;
MAT=zeros(length(Nsub),length(Ndh));    %Stability matrix

%Varying the inlet Enthalpy and calculating instability for whole range Ndh
for i=1:length(Nsub);
    clc
    fprintf('running... %0.2f %%',0.01.*round(10000.*(i-
1)./(length(Nsub).*1)));

    %Varying Ndh
    for k=1:length(Ndh);

        if Ndh(k)>Nsub(i);     %HIGH HEATING MODEL

            clear A B

            %ENTHALPY & SPECIFIC VOLUME STEADY STATE
            H0=0.5.*(Hin(i)+hpc);
            v0=specvol(H0);
            v0t=v0./vpc;
            L0=L.*Nsub(i)./Ndh(k);
            L0t=L0./L;
            L1=L-L0;
            L1t=L1./L;
            H1=hpc.*(1+Ndh(k).*L1./L);
            H1t=H1./(Ndh(k).*hpc);
            Hr=H1;

            v1=specvol(H1);
            v1t=v1./vpc;
            vr=v1;
            vrt=vr./vpc;
            Hint=Hin(i)./(Ndh(k).*hpc);
            H0t=H0./(Ndh(k).*hpc);
            Hrt=Hr./(Ndh(k).*hpc);
            hpct=1./Ndh(k);
```

```
T0=tmpr(H0);
T1=tmpr(H1);

%CALCULATING STEADY STATE MASS FLOW
f0=0.0316;
f1=0.0316;
fr=0.0316;
fd=0.0316;
Tw0=T0+1;
Tw1=T1+1;
ll0=thermc(H0);
ll1=thermc(H1);
Wtt=100;
dw=1;
it=0;

while dw>dwres;

     it=it+1;

    Wt=sqrt((g.*(area.^2).*L./(vpc.^2)).*((Ldt./vint(i)-
L0t./v0t-
(L1t+Lrt)./v1t)./(0.5.*((f0.*L0t./Dt+K0).*v0t+(fd.*Ldt./Dt+Kd).*vint(i))+0.
5.*(f1.*L1t./Dt+K1+fr.*Lrt./Dt+Kr).*v1t)));

    Re=Wt.*D./(area.*mu);
    f0=(0.316).*Re^(-1/4);
    f1=(0.316).*Re^(-1/4);
    fr=(0.316).*Re^(-1/4);
    fd=(0.316).*Re^(-1/4);

    Pr0=mu./ll0./(2*aa0*(H0-hpc)+1/cppc);
    Pr1=mu./ll1./(2*aa1*(H1-hpc)+1/cppc);
    rft0=specvol(H0)./specvol(enth(Tw0));
    rft1=specvol(H1)./specvol(enth(Tw1));
    Nu0=0.0069*Re^0.9*Pr0^0.66*rft0^0.43;
    Nu1=0.0069*Re^0.9*Pr1^0.66*rft1^0.43;

    conv0=Nu0.*ll0.*P_in.*L0./D;
    conv1=Nu1.*ll1.*P_in.*L1./D;
    cond=2.*llw.*Aw./L;
    qth=(Ndh(k).*Wt.*hpc.*L0t+conv0.*T0)./(conv0+cond);
    rth=cond/(conv0+cond);
    sth=(Ndh(k).*Wt.*hpc.*L1t+conv1.*T1)./(conv1+cond);
    tth=cond/(conv1+cond);
    Tw0=qth+rth.*Tw1;
    Tw1=sth+tth.*Tw0;

    L0=D.*Wt.*hpc.*Nsub(i)./Nu0./ll0./P_in./(Tw0-T0);
    L0t=L0./L;
    L1=L-L0;
    L1t=L1./L;

    H1=hpc+conv1.*(Tw1-T1)./Wt;
    T1=tmpr(H1);
    H1t=H1./(Ndh(k).*hpc);
    Hr=H1;
    Hrt=Hr./(Ndh(k).*hpc);
    v1=specvol(H1);
    v1t=v1./vpc;
```

```
                vr=v1;
                vrt=vr./vpc;

                ll0=thermc(H0);
                ll1=thermc(H1);

                dw=abs((Wtt-Wt)/Wt);
                Wtt=Wt;

                if it>itlim   %ITERATION WARNING
                    dw=0;
                    ie=ie+1;
                    Esub(ie)=Nsub(i);
                    Edh(ie)=Ndh(k);
                    warnstr{ie}=['warning at i=' num2str(i) ' k='
num2str(k) ' steady state calculations iteration limit exceeded'];
                end

                if k==2.*N./3
                    if i==1.*N./3
                        cvg(it)=dw;
                    end
                end


            end

            if Wt~=real(Wt); %IMAGINARY PART WARNING
                ie=ie+1;
                Esub(ie)=Nsub(i);
                Edh(ie)=Ndh(k);
                warnstr{ie}=['warning at i=' num2str(i) ' k=' num2str(k) '
nonreal flow, im/re=' num2str(imag(Wt)/real(Wt))];
            end

            if L0>L;    %LENGTH WARNING
                ie=ie+1;
                Esub(ie)=Nsub(i);
                Edh(ie)=Ndh(k);
                warnstr{ie}=['warning at i=' num2str(i) ' k=' num2str(k) '
length of node 0 exceeds L by ' num2str(round(-L1t.*10000)./100) ' %'];
            end

            %FROUDE NUMBER
            Nfr=(vpc.*Wt).^2./(g.*L.*area.^2);

            %DIMENSIONLESS VARIABLES
            T0t=T0.*llpc.*L./Ndh(k)./Wt./hpc;
            Tw0t=Tw0.*llpc.*L./Ndh(k)./Wt./hpc;
            T1t=T1.*llpc.*L./Ndh(k)./Wt./hpc;
            Tw1t=Tw1.*llpc.*L./Ndh(k)./Wt./hpc;
            aa1t=aa1.*hpc.*Ndh(k).*llpc.*L./Wt;
            aa0t=aa0.*hpc.*Ndh(k).*llpc.*L./Wt;
            cppct=cppc.*Wt./llpc./L;
            Cpwt=Cpw.*Wt./llpc./L;

            llwt=llw.*area./llpc./L.^2;
            ll0t=ll0./llpc;
            ll1t=ll1./llpc;
```

```
            Nu0dt=Nu0.*ll0t.^0.66;
            Nu1dt=Nu1.*ll1t.^0.66;
            bb1t=bb1.*Ndh(k).*hpc;

            %MATRICES A & B
            A(1,1)=(H0t./hpct-1)./v0t;
            A(2,1:2)=[1./v1t-H0t./(hpct.*v0t) -
L1t.*(C.*hpc./vpc).*Ndh(k)./(v1t.^2)];
            A(3,3)=-Lrt.*Ndh(k).*(C.*hpc./vpc)./(vrt.^2);
            A(4,1:2)=[H1t./v1t-H0t./v0t (L1t./v1t).*(1-
Ndh(k).*(C.*hpc./vpc).*H1t./v1t)];
            A(5,3)=(Lrt./vrt).*(1-Ndh(k).*(C.*hpc./vpc).*Hrt./vrt);
            A(6,4:6)=[(1-L1t+Ldt+Vbt) L1t Lrt];

            A(7,1)=-rrwt.*Cpwt.*Awt.*Tw0t;
            A(7,7)=rrwt.*Cpwt.*Awt.*L0t;
            A(8,1)=rrwt.*Cpwt.*Awt.*Tw1t;
            A(8,8)=rrwt.*Cpwt.*Awt.*L1t;

            B(1,1:4)=[1./hpct 0 0 1-Hint./hpct];
            B(2,1:5)=[-1./hpct 0 0 Hint./hpct -1];
            B(3,5:6)=[1 -1];

            B(4,1)=P_int./Dt.*(Nu1dt.*ll1t.^0.34.*(Tw1t-T1t)-
Nu0dt.*ll0t.^0.34.*(Tw0t-T0t));
            B(4,2)=-1-Nu1dt.*P_int.*L1t./Dt.*((2.*aa1t.*(H1t-
hpct)+1./cppct).*ll1t.^0.34+0.34.*(Tw1t-T1t).*ll1t.^-
0.66.*bb1t.*llzt.*exp(-bb1.*H1));
            B(4,3:5)=[0 Hint -H1t];
            B(4,7:8)=[Nu0dt.*ll0t.^0.34.*P_int.*L0t./Dt
Nu1dt.*ll1t.^0.34.*P_int.*L1t./Dt];

            B(5,2:6)=[1 -1 0 H1t -Hrt];
            B(6,1)=0.5.*(f0.*v0t./Dt-f1.*v1t./Dt)+1./(Nfr.*v0t)-
1./(Nfr.*v1t);
            B(6,2)=Ndh(k).*(C.*hpc./vpc).*(-
0.5.*(f1.*L1t./Dt+K1)+L1t./(Nfr.*(v1t.^2)));
            B(6,3)=Ndh(k).*(C.*hpc./vpc).*(-
0.5.*(fr.*Lrt./Dt+Kr)+Lrt./(Nfr.*(vrt.^2)));
            B(6,4)=-((f0.*L0t./Dt+K0).*v0t+(fd.*Ldt./Dt+Kd).*vint(i)-
vint(i));
            B(6,5)=-v1t.*(f1.*L1t./Dt+K1);
            B(6,6)=-vrt.*(fr.*Lrt./Dt+Kr+vint(i)./vrt);
            B(7,1)=Nu0dt.*ll0t.^0.34.*P_int./Dt.*(Tw0t-T0t)-1;
            B(7,7)=-Nu0dt.*ll0t.^0.34.*P_int.*L0t./Dt-2.*llwt.*Awt;
            B(7,8)=2.*llwt.*Awt;
            B(8,1)=1-Nu1dt.*ll1t.^0.34.*P_int./Dt.*(Tw1t-T1t);
            B(8,2)=Nu1dt.*P_int.*L1t./Dt.*((2.*aa1t.*(H1t-
hpct)+1./cppct).*ll1t^0.34+0.34.*(Tw1t-T1t).*ll1t.^-0.66.*bb1t.*llzt.*exp(-
bb1.*H1));
            B(8,7)=2.*llwt.*Awt;
            B(8,8)=-Nu1dt.*ll1t.^0.34.*P_int.*L1t./Dt-2.*llwt.*Awt;

        else        %LOW HEATING MODEL

            clear A B

            %ENTHALPY & SPECIFIC VOLUME STEADY STATE
            CC=C2.*Ndh(k).*hpc.*vpc;
            Hint=Hin(i)./(Ndh(k).*hpc);
```

```
            Hout=Hin(i)+Ndh(k).*hpc;
            Houtt=Hout./(Ndh(k).*hpc);
            H0=0.5.*(Hin(i)+Hout);
            H0t=H0./(Ndh(k).*hpc);
            Hr=Hout;
            Hrt=Houtt;
            hpct=1./Ndh(k);

            vout=specvol(Hout);
            voutt=vout./vpc;
            v0=specvol(H0);
            v0t=v0./vpc;
            vr=vout;
            vrt=vr./vpc;

            T0=tmpr(H0);

            %CALCULATING STEADY STATE MASS FLOW
            f0=0.0316;
            fr=0.0316;
            fd=0.0316;
            Tw=T0+1;
            Wtt=100;
            dw=1;
            it=0;
            ll0=thermc(H0);

            while (dw>dwres);

                Wt=sqrt((g.*(area.^2).*L./(vpc.^2)).*((Ldt./vint(i)-1./v0t-
Lrt./vrt)./(0.5.*((f0./Dt+K0).*v0t+(fd.*Ldt./Dt+Kd).*vint(i))+0.5.*(fr.*Lrt
./Dt+Kr).*vrt)));
                Re=Wt.*D./(area.*mu);
                f0=(0.316).*Re^(-1/4);
                fr=(0.316).*Re^(-1/4);
                fd=(0.316).*Re^(-1/4);

                Pr0=mu./ll0./(2*aa0*(H0-hpc)+1/cppc);
                rft0=specvol(H0)./specvol(enth(Tw));
                Nu0=0.0069*Re^0.9*Pr0^0.66*rft0^0.43;
                conv0=Nu0.*ll0.*P_in.*L./D;

                Tw=Ndh(k).*Wt.*hpc./conv0+T0;
                Hout=Hin(i)+conv0./Wt.*(Tw-T0);
                H0=0.5.*(Hin(i)+Hout);
                T0=tmpr(H0);

                H0t=H0./(Ndh(k).*hpc);
                Houtt=Hout./(Ndh(k).*hpc);
                Hr=Hout;
                Hrt=Houtt;
                hpct=1./Ndh(k);

                vout=specvol(Hout);
                voutt=vout./vpc;
                v0=specvol(H0);
                v0t=v0./vpc;
                vr=vout;
                vrt=vr./vpc;
```

```
                ll0=thermc(H0);

                dw=abs((Wtt-Wt)/Wt);
                Wtt=Wt;
                it=it+1;
                                if k==2.*N./3
                    if i==1.*N./3
                        cvg(it)=dw;
                    end
                end

                if it>itlim   %ITERATION WARNING
                    dw=0;
                    ie=ie+1;
                    Esub(ie)=Nsub(i);
                    Edh(ie)=Ndh(k);
                    warnstr{ie}=['warning at i=' num2str(i) ' k='
num2str(k) ' steady state calculations iteration limit exceeded'];
                end
            end

            if Hout>hpc %ENTHALPY WARNING
                ie=ie+1;
                Esub(ie)=Nsub(i);
                Edh(ie)=Ndh(k);
                warnstr{ie}=['warning at i=' num2str(i) ' k=' num2str(k) '
enthalpy at exit of node 0 exceeds hpc by ' num2str(round(10000.*(Hout-
hpc)/hpc)./100) ' %'];
            end


            %DIMENSIONLESS VARIABLES
            T0t=T0.*llpc.*L./Ndh(k)./Wt./hpc;
            Twt=Tw.*llpc.*L./Ndh(k)./Wt./hpc;
            aa0t=aa0.*hpc.*Ndh(k).*llpc.*L./Wt;
            cppct=cppc.*Wt./llpc./L;
            Cpwt=Cpw.*Wt./llpc./L;

            llwt=llw.*area./llpc./L.^2;
            ll0t=ll0./llpc;
            Nu0dt=Nu0.*ll0t.^0.66;
            bb0t=bb0.*Ndh(k).*hpc./llpc;

            %FROUDE NUMBER
            Nfr=(vpc.*Wt).^2./(g.*L.*area.^2);

            %MATRICES A & B
            A(1,1:2)=[0.5.*CC Lrt.*CC];
            A(2,1:2)=[0.5./v0t+0.5.*H0t.*CC Houtt.*Lrt.*CC];
            A(3,2)=Lrt./vrt+Lrt.*CC.*(Hrt-Houtt);
            A(4,3:4)=[(1+Vbt+Ldt) Lrt];
            A(5,5)=rrwt.*Cpwt.*Awt;

            B(1,3:4)=[1 -1];
            B(2,1)=-1-(Nu0dt.*P_int./Dt.*(ll0t.^0.34.*(aa0t.*(H0t-
hpct)+.5./cppct)+0.17.*ll0t.^-0.66.*(Twt-T0t).*bb0t));
            B(2,2:4)=[0 Hint -Houtt];
            B(2,5)=Nu0dt.*ll0t.^0.34.*P_int./Dt;
```

```
            B(3,1:4)=[1 -1 0 Houtt-Hrt];
            B(4,1)=0.25.*(f0./Dt+K0).*CC.*v0t.^2-CC./(2.*Nfr);
            B(4,2)=0.5.*(fr.*Lrt./Dt+Kr).*CC.*vrt.^2-CC.*Lrt./Nfr;
            B(4,3)=-(fd.*Ldt./Dt+Kd).*vint(i)-(f0./Dt+K0).*v0t+vint(i);
            B(4,4)=-(fr.*Lrt./Dt+Kr).*vrt-vint(i);
            B(5,1)=Nu0dt.*P_int./Dt.*(ll0t.^0.34.*(aa0t.*(H0t-
hpct)+.5./cppct)+0.17.*ll0t.^-0.66.*(Twt-T0t).*bb0t);
            B(5,5)=-Nu0dt.*ll0t.^0.34.*P_int./Dt;

        end



        %Calculation of (un)stable points
        if
(mean(mean(isnan(A)))~=0||mean(mean(isnan(B)))~=0||mean(mean(isinf(A)))~=0|
|mean(mean(isinf(B)))~=0) %NaN and Inf warnings
            A(isnan(A))=1;
            B(isnan(B))=1;
            A(isinf(A))=10^99;
            B(isinf(B))=10^99;
            ie=ie+1;
            Esub(ie)=Nsub(i);
            Edh(ie)=Ndh(k);
            warnstr{ie}=['warning at i=' num2str(i) ' k=' num2str(k) ' NaN
or Inf'];
        end

        [V,E]=eig(B,A);             %Calculating eigenvalues
        E(abs(E)>1e12)=0;           %Filtering the infinite eigenvalues
that don't contribute
        lab=real(diag(E));
        lab1=(lab>0);

        if mean(lab1)>0
            MAT(i,k)=0; %Instable point
        else
            MAT(i,k)=1; %Stable point
        end
    end

end


%Instability plot
RB=[1 0 0; 0 0 1];
hold on
imagesc(Ndh,Nsub,MAT);
colormap(RB);
set(gca,'YDir','normal');
xlabel('N_\Delta_h', 'Fontsize',16);
ylabel('N_s_u_b', 'Fontsize',16);

axis equal
axis tight

% COMPOSE ERROR LOG
clc
```

```
TD=round(clock);
disp('STABILITY MAP');
disp('SYSTEM PARAMETERS');
L,area,Lr,Vb,D,P_in,Aw,rrw,Cpw,llw
disp('FRICTION COEFFICIENTS');
K0,K1,Kr,Kd
disp(['RESOLUTION = ', num2str(N)]);

fprintf('log generated on %04d-%02d-%02d at %02d:%02d:%02d
\n',TD(1),TD(2),TD(3),TD(4),TD(5),TD(6));

if ie>0
    for iei=1:ie;
        disp(warnstr{iei});
    end
end

hold off
toc
```

D.2. Function with input spec. enthalpy and output specific volume at *P*=25MPa

```
function [v1] = specvol(H1)
%Calculation of specific volume with H1 (Krijger)
C=0.80e-8;
vpc=3.1564e-3; %2.5843e-3;
hpc=2.1529e6; %2033.e3;
v11=1.2326e-3;
h11=1.1201e6;
rho=1./v11+((1./vpc-1./v11)./(hpc-h11)).*(H1-h11);

for kk=1:length(H1);
    if H1(kk)<hpc;
        v1(kk)=1./rho(kk);
    else (H1(kk)>=hpc);
        v1(kk)=vpc+C.*(H1(kk)-hpc);
    end
end

end
```

D.3. Function with input spec. enthalpy and output temperature at *P*=25MPa

```
function [T1] = tmpr(H1)
% Calculation of temperature with specific enthalpy H1
Tpc = 384.89;
cp = 76.444e3;
hpc = 2152.2e3;
A0=-1.1e-10;
A1=1e-10;
h1=H1-hpc;

for kk=1:length(h1);
    if h1(kk)<0;
        T1(kk)=A0*h1(kk)^2+h1(kk)/cp+Tpc;
    else h1(kk)>=0;
        T1(kk)=A1*h1(kk)^2+h1(kk)/cp+Tpc;
```

```
    end
end
end
```

D.4. Function with input spec. enthalpy and output thermal conductivity at *P*=25MPa

```
function [ll0] = thermc(H0)
bb0=-3.2711e-7;
llb0=1.0133;
llb1=0.070154;
llz=4.555298930195932;
bb1=1.369367779861587e-06;
hpc=2.1529e6;
ll0=zeros(1,length(H0));
for iii=1:length(H0);
    if H0(iii)<hpc;
        ll0(iii)=bb0.*H0(iii)+llb0;
    else
        ll0(iii)=llb1+llz.*exp(-bb1.*H0(iii));
    end
end
end
```

D.5. Function with input temperature and output specific enthalpy at *P*=25MPa

```
function [H1] = enth(T1)
% Calculation of enthalpy with temperature T1
Tpc = 384.89;
cp = 76.444e3;
hpc = 2152.2e3;
A0=-1.1e-10;
A1=1e-10;

for kk=1:length(T1);
    if T1(kk)>=Tpc;
        H1(kk)=hpc+(.5/A1)*(-1/cp+sqrt(1/cp^2-4*A1*(Tpc-T1(kk))));
    else T1(kk)<Tpc;
        H1(kk)=hpc+(.5/A0)*(-1/cp+sqrt(1/cp^2-4*A0*(Tpc-T1(kk))));
    end
end
end
```